Aus dem Exzellenzcluster NeuroCure der Medizinischen Fakultät
Charité – Universitätsmedizin Berlin

DISSERTATION

Advanced Retinal Optical Coherence Tomography Image Analysis in Neuroinflammatory Disorders

zur Erlangung des akademischen Grades

Doctor rerum medicinalium (Dr. rer. medic.)

vorgelegt der Medizinischen Fakultät
Charité – Universitätsmedizin Berlin

von

Seyedamirhosein Motamedi

aus Teheran, Iran

Datum der Promotion: 04.06.2021

For all those who have been deprived of their right to education

Table of Contents

Synopsis

Abstract

Retinal optical coherence tomography (OCT) is a promising biomarker for disease monitoring in neurodegenerative and neuroinflammatory disorders. Multiple sclerosis (MS) and neuromyelitis optica spectrum disorders (NMOSD) affect the retina as a result of retrograde neurodegeneration, mainly after optic neuritis (ON), but potentially also from ON-independent primary retinal pathology. However, traditional OCT analysis methods might be insufficient to detect subtle retinal changes.

The objective of this work was to optimize image analysis of macular OCT images using two parallel approaches: 1) developing a semi-automated intraretinal segmentation pipeline for macular OCT images and introducing minimally detectable changes, based on intra-rater reliability of manual correction of segmentation, and normative data for different retinal layers in healthy controls (HCs) [*Normative-Data*], and 2) introducing a novel method to characterize the shape of the fovea by several parameters [*Foveal-Shape-Method*] and investigating foveal shape changes in NMOSD patients compared to MS patients and HCs [*NMOSD-Foveal-Shape*].

Normative-Data showed that total macular, macular retinal nerve fiber layer, combined ganglion cell and inner plexiform layer (GCIPL) and inner nuclear layer thicknesses have significant negative correlation with age in HCs. Total macular and GCIPL thicknesses showed significantly higher values in males compared to females. The calculated minimally detectable changes in normative data were considerably higher than typical annual changes caused by neurodegeneration in neuroinflammatory disorders, but lower than damage typically seen in ON. *Foveal-Shape-Method* describes the foveal shape from the foveal pit to the parafoveal points with the maximum heights using 19 parameters. *NMOSD-Foveal-Shape* showed that a majority of the foveal shape parameters were significantly different in NMOSD but not in MS patients in comparison to HCs. The parameters describing the foveal pit flatness and the steepest part of the fovea and the Inner Rim Volume showed an area under the curve of 0.7 or better in discriminating NMOSD and MS and were significantly different between NMOSD and MS, regardless of ON status.

To summarize, intraretinal layer segmentation using currently available OCT images is not sufficient to detect typical thickness changes from progressive neurodegeneration. However, intraretinal layer segmentation is able to measure changes caused by inflammatory damage, i.e. ON, which are typically magnitudes higher. The *NMOSD-Foveal-Shape* results indicate a primary retinopathy in NMOSD, possibly as a result of damage to aquaporin-4-expressing Müller cells in the fovea. The results can improve the application of OCT and will thus potentially open new avenues to better understand and potentially develop treatments for NMOSD.

Abstrakt

Die retinale optische Kohärenztomographie (OCT) ist ein vielversprechender Biomarker bei neurodegenerativen und neuroinflammatorischen Erkrankungen. Multiple Sklerose (MS) und Neuromyelitis optica-Spektrum-Erkrankungen (NMOSD) betreffen die Netzhaut infolge retrograder Neurodegeneration, hauptsächlich nach einer Neuritis nervi optici (ON), möglicherweise aber auch aufgrund einer ON-unabhängigen primären Netzhautpathologie. Herkömmliche OCT-Analysemethoden sind jedoch möglicherweise unzureichend, um solche subtilen Veränderungen nachzuverfolgen.

Das Ziel dieser Arbeit war es, die Bildanalyse von OCT-Bildern der Makula unter Verwendung von zwei parallelen Ansätzen zu optimieren: 1) Entwicklung einer halbautomatischen intraretinalen Segmentierungspipeline für OCT-Bilder der Makula und Einführung minimal nachweisbarer Änderungen, basierend auf der Intra-Rater-Zuverlässigkeit der manuellen Korrektur der Segmentierung, und normativer Daten für verschiedene Netzhautschichten in gesunden Kontrollen (GK) [*Normative-Daten*] und 2) Einführung einer neuartigen Methode zur Charakterisierung der Morphometrie der Fovea durch verschiedene Parameter [*Foveal-Shape-Method*] und Untersuchung morphometrischer fovealer Veränderungen bei NMOSD-Patienten im Vergleich zu MS-Patienten und GK [*NMOSD-Foveal-Shape*].

Die *Normative-Daten* Studie zeigte, dass die Dicke der gesamten Makula, der makularen retinalen Nervenfaserschicht, der kombinierten Ganglienzell- und inneren plexiformen Schicht (GCIPL) und der inneren Körnerzellschicht eine signifikante negative Korrelation zum Alter bei GKs aufweist. Die Gesamtdicke von Makula und GCIPL zeigte bei Männern signifikant höhere Werte als bei Frauen. Die berechneten minimal nachweisbaren Änderungen der normativen Daten waren erheblich höher als die typischen jährlichen Änderungen, die durch Neurodegeneration bei neuroinflammatorischen Erkrankungen verursacht wurden.

Die *Foveal-Shape-Method* Studie beschreibt die Form der Fovea von der Fovealgrube bis zu den Parafovealpunkten mit den maximalen Höhen unter Verwendung von 19 Parametern. *NMOSD-Foveal-Shape* zeigte, dass ein Großteil der fovealen Formparameter bei NMOSD signifikant unterschiedlich war, bei MS-Patienten jedoch nicht im Vergleich zu GKs. Die Parameter, die die Ebenheit der Fovealgrube und den steilsten Teil der Fovea beschreiben sowie das innere Randvolumens zeigten eine Fläche unter der Kurve von 0,7 oder besser bei der Unterscheidung von NMOSD und MS und unterschieden sich zwischen NMOSD und MS unabhängig vom ON-Status signifikant.

Zusammenfassend lässt sich sagen, dass die intraretinale Schichtsegmentierung unter Verwendung derzeit verfügbarer OCT-Bilder typische Dickenänderungen aufgrund einer fortschreitenden Neurodegeneration nur unzureichend erkennen kann. Die intraretinale Schichtsegmentierung kann jedoch Änderungen messen, die durch entzündliche Schäden wie im Rahmen einer ON verursacht werden, die typischerweise um Größenordnungen höher sind. Die *NMOSD-Foveal-Shape*-Ergebnisse zeigen eine primäre Retinopathie bei NMOSD, jedoch nicht

bei MS, möglicherweise als Folge einer Schädigung von Aquaporin-4-exprimierenden Müller-Zellen in der Fovea. Die Ergebnisse können die Anwendung von OCT verbessern und so möglicherweise neue Wege eröffnen, um NMOSD besser zu verstehen und möglicherweise neue Therapieansätze zu entwickeln.

Introduction

Multiple sclerosis (MS) is the most common autoimmune disorder of the central nervous system (CNS) [1]. The exact etiology of MS is unknown, but central element is an immune system dysregulation by infiltration of autoreactive lymphocytes to CNS, which causes inflammation in different regions of the brain and spinal cord and subsequently results in demyelination, axonal injury, and eventually neuronal loss. It is known that MS is more common in women than men (more than 3:1) and disease onset occurs in young adulthood [1]. The most common form of MS is relapsing-remitting multiple sclerosis (RRMS) which is characterized by attacks lasting for a period of days to months followed by complete or partial recovery [2].

Neuromyelitis optica spectrum disorders (NMOSD) are an important differential diagnosis of MS with rarer incidence. NMOSD are autoimmune inflammatory disorders of the CNS, which predominantly affect optic nerves and spinal cord causing attacks such as ON and transverse myelitis [3]. Approximately 80% of patients with NMOSD are tested positive for serum autoantibody against aquaporin-4 (AQP4), an astrocytic water channel [4,5]. NMOSD typically shows first symptoms in the age-range of 35-45 with a much higher incidence in women compared to men, especially in AQP4-IgG-seropositive patients (up to 10:1) [5,6]. Up to 90% of NMOSD patients show a relapsing disease course, while the rest show a monophasic course or, in very rare cases, a progressive course [6]. Thanks to the discovery of AQP4-IgG, there have been several hypotheses suggested for the pathogenesis of AQP4-IgG-seropositive NMOSD patients. One hypothesis is that AQP4-IgG infiltrates the CNS and binds to AQP4-expressing water channels on astrocytes and activates complement cascade that subsequently results in astrocyte and oligodendrocyte death, demyelination, and finally neural loss [7]. Additionally, a hypothesis for a complement independent astrocytic injury by AQP4-IgG binding to the water channels causing water homeostasis disruption has been suggested [8].

The vast majority of MS patients experience ON, either as their first symptom (around 25%) or later during the disease course (around 70%) [9]. ON is the most common first symptom in NMOSD patients (about 55%), often with bilateral involvement with more severe visual impairment, higher lesion extent, and retinal damage compared to MS patients with ON [10,11]. Clinically, ON can be divided to typical and atypical forms, with the typical form being unilateral with moderate visual acuity loss, pain, color desaturation, and often associated with MS, and the atypical form being bilateral with strong ONH edema, more visual acuity loss, and often associated with NMOSD [9,12].

The retina as a part of the CNS is affected in MS and NMOSD, mainly as a result of retrograde neurodegeneration related to ON but potentially also attack-independent primary retinal pathology. The retina is separated from the vitreous body by the inner limiting membrane (ILM) and ends at the Bruch's membrane, the innermost layer of the choroid. The retina has two prominent anatomical landmarks: 1) the macula where the light is focused on and is responsible for high resolution color vision, and 2) the optic nerve head, where the axons of retinal ganglion

cells form the optic nerve and exit the retina [13]. The central part of the macula is referred to as the fovea, which is densely packed with photoreceptors and provides high acuity vision. The retina consists of photoreceptors that convert light to signals, bipolar cells that transmits the signal from photoreceptors to ganglion cells, and ganglion cells that carry the signal from the retina to the brain. There are other nerve cells in the macula, namely amacrine cells, which affect the output from bipolar cells, and horizontal cells, which regulates the output from photoreceptors [13]. In addition to neurons, there are three types of glial cells in the retina: Müller cells, which are the major glial cells in the retina and the only type present near the fovea, astrocytes and microglia. Müller cells, which are AQP4-expressing, span the entire thickness of the retina and have several crucial roles in maintaining the health and functionality of the retina and its neurons, such as supporting the physical structure of the retina, regulating the blood flow, maintaining the homeostasis of water, ions and neurotransmitters in the retinal extracellular matrix, and enhancing the transmission of light to photoreceptors [14]. Astrocytes, which are also AQP4-expressing, are located in the retinal nerve fiber layer, with a symmetrical stellate form in peripheral retina and an elongated form near the optic nerve [15]. Astrocytes and Müller cells' end-feet form the ILM.

Optical coherence tomography (OCT) is a fast, non-invasive, high resolution imaging technique, which can be used to generate three-dimensional images of the retina [16]. Since its introduction and first applications in retinal imaging in the 90s, retinal OCT has evolved as a standard tool to quantify neurodegeneration and inflammation in patients with CNS autoimmune disorders and to improve the understanding of disease mechanisms in these patients [12,17]. Retinal OCT research has been moving more towards harmonization by adaptation of consensus criteria such as OSCAR-IB for scan quality [18] and APOSTEL for reporting [19], which have been introduced in recent years.

Since the first application of retinal OCT, many studies have investigated peripapillary retinal nerve fiber layer (pRNFL) changes in MS and NMOSD [12,17]. pRNFL is mostly calculated as an average thickness of unmyelinated axons of ganglion cells in a circular OCT scan around the optic nerve head. While being in the anterior part of the afferent visual system, pRNFL is considered to be a standard biomarker to assess and monitor retrograde retinal damage from ON and lesions in the posterior visual pathway [12,17]. Studies have shown significant thinning in pRNFL of MS, and to a higher extent, NMOSD eyes with a history of ON (ON+) [20]. Although pRNFL has become a standard OCT biomarker for assessment of retinal damage, it shows swelling in acute phase of ON and thus should not be used as biomarker for neurodegeneration up to 3 months after an acute ON attack [21]. Another drawback is that blood vessels pass through pRNFL and therefore can affect the thickness measurements, especially in cases where the thickness is greatly reduced in severely affected eyes [22].

Since the introduction and wide implementation of spectral-domain OCT (SD-OCT), which produces high definition 3D images of the macula, the combined ganglion cell and inner plexiform layer (GCIPL) has gained more attention and is sought to complement or even replace the

conventional pRNFL measurement for neuro-axonal retinal damage [12,17]. The ganglion cell layer, where the cell body of the majority of ganglion cells are located, is often combined with the inner plexiform layer, where the ganglion cell dendrites and amacrine and bipolar cell axons are located, due to similar reflectivity in OCT images, which makes discriminating the two layers with the current OCT technology difficult [23]. GCIPL showed significant thinning in eyes affected by ON in MS and NMOSD [20,24], even in eyes with acute ON episodes [25]. Reduction in the thickness of pRNFL and GCIPL is not limited to eyes affected by ON. Studies have shown thinning in pRNFL and GCIPL of MS eyes without a previous history of optic neuritis (ON-) compared to healthy controls (HC) [24,25], suggestive of subclinical disease activity, while studies in NMOSD ON- eyes show conflicting results, with some showing thinning in pRNFL or GCIPL and others showing no significant changes [12]. OCT parameters have been shown to be predictive of inflammatory disease activity. Martinez-Lapiscina et al. showed that MS patients with pRNFL thickness equal to or lower than 87 µm at baseline had a higher risk of disability worsening in a period of one year to three years of follow-up [26]. Zimmermann & Knier et al. also showed that, in clinically isolated syndrome (CIS), a clinical condition with a monophasic attack with features suggestive of MS, ON- patients with GCIPL thickness in the lowest tertile had a four times higher risk of being diagnosed with MS in the follow-up [27]. The inner nuclear layer (INL), which is compromised of the cell body of bipolar, horizontal and amacrine cells, displayed thickening in ON+ eyes in NMOSD and MS [28], related to inflammatory activity in MS patients [29,30].

In 2016, Jeong et al. reported thinning in foveal thickness, the thickness of the macula in an area of half a millimeter in radius around the center, in AQP4-IgG-serpositive patients regardless of the history of ON compared to healthy controls, in contrast to pRNFL, which only showed thinning in ON+ eyes [31]. Oertel and Kuchling et al. confirmed this by showing foveal thinning in AQP4-IgG seropositive NMOSD ON+ and ON- patients, in an exploratory and a confirmatory cohort, in comparison to HCs, in contrast to pRNFL and GCIPL thinning, which was reported only in ON+ patients [32]. Oertel and Kuchling et al. also showed a subjective shape change in the fovea from a V-shape in healthy eyes to flattened U-shape in NMOSD eyes. These findings are suggestive of retinal shape changes specific to AQP4-IgG-seropositive NMOSD, which might be linked to AQP4-IgG. Studies on rats have shown complement independent AQP4 loss in Müller cells exposed to AQP4-IgG, which supports the hypothesis of an AQP4-IgG-mediated primary retinopathy in NMOSD [33,34]. Autopsy in AQP4-IgG-seropositive NMOSD patients has been also suggestive of AQP4-IgG-mediated primary retinal damage [35].

Given the background and recent findings, the need to examine the shape of the fovea in an objective and quantitative manner is increasingly apparent. Using layer thicknesses and volumes might also eliminate and hide some important and relevant retinal changes in patients with neurodegenerative and neuroinflammatory disorders of CNS and therefore undermine the potentials of retinal OCT research in these disorders. Besides, more studies are needed to establish normative values for intraretinal layers in different populations and OCT devices, to

investigate the relation of intraretinal layer thicknesses to parameters like age and sex, and to determine the amount of noise induced by different factors such as inter-rater and intra-rater differences in manual correction of segmentation boundaries, which are essential to interpret observed retinal changes in patients. Additionally, although there has been huge improvement in the accuracy of intraretinal layer segmentation, a toolbox to facilitate the whole process from reading and examining to segmenting, manually correcting, and data exporting of OCT devices is lacking. The aim of this work was to move towards overcoming the challenges in OCT image analysis by introducing and applying novel advanced image analysis methods to better understand retinal changes in autoimmune disorders, by:

1. Developing a new adaptable pipeline for semi-automated intraretinal OCT segmentation and establishing normative data and minimally detectable changes for inner retinal thicknesses in a healthy Caucasian population, referred to as *Normative-Data* throughout this synopsis [36].
2. Introducing and validating a 3D foveal shape analysis method, referred to as *Foveal-Shape-Method* throughout this synapsis [37].
3. Investigating foveal shape changes in AQP4-IgG-seropositive NMOSD patients using the introduced foveal shape analysis method and comparing with findings in MS patients and healthy controls, referred to as *NMOSD-Foveal-Shape* throughout this synopsis [38].

Materials and Methods

Study population

All the participants included in the studies of this work were recruited at NeuroCure Clinical Research Center of Charité - Universitätsmedizin Berlin. The studies were approved by the local ethics committee at Charité - Universitätsmedizin Berlin (EA1/131/09, EA1/163/12, EA1/182/10). The confirmatory data in *NMOSD-Foveal-Shape* was collected under approval from the local ethics committee at Heinrich-Heine University Düsseldorf. We adhered to the declaration of Helsinki in its currently applicable version and the applicable German and European laws in conducting the studies. All participants gave written informed consent.

For *Normative-Data* [36], we retrospectively analyzed macular OCT scans of healthy controls in two multimodal register studies who visited our center between July 2010 and March 2018. The inclusion criteria were healthy conditions with the age between 18 to 70 with Caucasian ethnicity and macular OCT of both eyes (eyes with low quality OCT scans were excluded from the analysis). The exclusion criteria were any neurological conditions, and any pathological conditions known to affect eyes. After applying these criteria, macular OCT scans of 423 eyes of 218 HCs (144 (66%) females) with a mean age (± standard deviation (SD)) of 36.5 (± 12.3) years were included in the analysis. To test inter-rater reliability in manually correcting boundaries segmentation, the segmentation of macular OCT of 44 eyes of 24 HCs was manually corrected, if needed, by two masked experienced raters. The same number of OCT scans were manually

corrected by a single rater twice to measure intra-rater reliability. Additionally, high quality OCT scans of 20 NMOSD ON+ eyes were included for performance assessment of the segmentation pipeline [36].

For *NMOSD-Foveal-Shape* [38], data from an ongoing observational cohort study of our center on patients with NMOSD were included retrospectively. The inclusion criteria were a minimum of age of 18 and fulfillment of the diagnostic criteria for AQP4-seropositive patients according to the revised diagnostic criteria for NMOSD (2015) [39]. The exclusion criteria were any other neurological disorder or any ophthalmological disorder known to affect the eyes. Eyes of patients with an ON episode up to six months prior to the OCT exam were not included in this study. OCT scans of 56 eyes from 28 AQP4-IgG-seropositive patients (26 (93%) women, 20 (38%) ON+ eyes, mean age of 43.6 (± 11.5) years) were included in this study after applying the inclusion and exclusion criteria. 116 eyes from 60 relapsing-remitting MS patients and 123 eyes from 62 healthy controls from different cohort studies of our center, age and sex matched with the NMOSD cohort were also included in this study. A confirmatory cohort with macular OCT scans of 58 eyes from 33 AQP4-IgG-seropositive patients and 62 eyes from 33 MS patients were included from Düsseldorf. The proportion of eyes with ON between NMOSD and MS patients were matched in the exploratory cohort but were significantly different in the confirmatory cohort ($p = 0.001$) [38]. For more details on study population, please see the respective publications [36,38].

Optical coherence tomography

OCT images are formed from backscattering near infrared light from tissues, which is interfered with using a reference beam to measure depth and relative intensity and therefore form 2D cross sectional or 3D volumetric images [40]. Volumetric OCT images are composed of parallel cross-sectional scans called B-scans. Each B-scan is comprised of several axial scans or A-scans. It was the introduction and adaptation of spectral-domain OCT (SD-OCT), which uses a broad-band light source and a spectrometer to measure the reflectivity that boosted its use in medical imaging. SD-OCT offers high axial resolution (3-5 µm), high signal to noise ratio due to image averaging, and fast image acquisition (typical A-scan rate of 40 kHz) [41].

All OCT scans for the studies in this work were acquired using Spectralis SD-OCT from Heidelberg Engineering (Heidelberg, Germany), with automatic real time (ART) averaging and active eye tracking. Macular volume scans were taken in a 25°×30° area around the fovea (61 vertical B-scans, 768 A-scans per B-scan, ART of 15) and peripapillary ring scans were taken in a 12° circle around the optic nerve head (single B-scan with 1536 A-scans, $16 \leq \text{ART} \leq 100$). The thickness of pRNFL is reported as the average thickness in µm in peripapillary ring scans. The thickness of the macula (total macular thickness), macular retinal nerve fiber layer (mRNFL), GCIPL, and INL are reported as average thickness in µm or volume in mm^3 in a 6 millimeter diameter around the fovea and FT is reported as the average thickness or volume in a 1 mm diameter around the fovea. The analysis of intraretinal layers in different sectors of the Early Treatment Diabetic Retinopathy Study (ETDRS) [42] macular map was also included in

Normative-Data as supplementary materials. The segmentation, review for quality control, manual correction of segmentation boundaries and thickness data export of OCT images were done using Heidelberg Engineering Eye Explorer (HEYEX 1.9.10.0) for *NMOSD-Foveal-Shape* and with a custom-developed segmentation pipeline (SAMIRIX) for *Normative-Data*. All OCT scans were quality controlled according to the OSCAR-IB criteria [18] and OCT data was reported in accordance with the APOSTEL recommendations [19].

Statistical analysis

Regression analysis was based on linear mixed-effect models (LMM) for *Normative-Data* and *NMOSD-Foveal-Shape* with inter-eye within-patient correlations as a random factor to correct for two eyes per patient. For *NMOSD-Foveal-Shape*, LMM additionally had age and sex as random factors. The conditional and marginal coefficients of determination for linear regression were calculated based on pseudo R-squared. P-values in *NMOSD-Foveal-Shape* were corrected for multiple testing using the Benjamini-Hochberg procedure. For confirmatory cohort of *NMOSD-Foveal-Shape*, one-sided p-values were reported, without multiple testing correction. Correlation analysis was performed using Pearson's product-moment correlation. Sex and ON differences between groups were assessed using a chi-squared test. Age differences were assessed using two-sample Wilcoxon test. Intra-class correlation (ICC) coefficients and 95% confidence intervals were calculated based on the variance components of a one-way ANOVA. The minimum detectable change (MDC), used to measure the noise induced by intra-rater and inter-rater differences in *Normative-Data*, was calculated based on the formulas suggested by Beckerman et al. [43]. Area under the curve (AUC) from receiver operating characteristic (ROC) curves was reported for performance analysis. Stepwise logistic regression was based on generalized linear models and Akaike's Information Criteria with both backward and forward modes of stepwise search. All statistical analysis of the studies of this work were done in R with version 3.4.4 or 3.5.0 (The R Project for Statistical Computing, https://www.r-project.org), using stats, lme4, lmerTest, MuMIn, ROCR, ggplot2, ICC, plotROC, pwr, multcomp, and ggpubr packages. P-values below 0.05 were considered significant.

Data availability

The survey tool and all data used for *Normative-Data* as well as the SAMIRIX toolbox were published open-source with the publication and on other repositories. The publication of the data was in line with the General Data Protection Regulation and other applicable European and German laws and approved by the Administrative Office for Data Protection at Charité - Universitätsmedizin Berlin.

Results

Segmentation pipeline (SAMIRIX)

Normative-Data [36]

SAMIRIX is a custom segmentation pipeline that interchangeably adapts a third-party segmentation algorithm and provides a complete pipeline for reading OCT images, batch segmentation, reviewing and manually correcting the segmentation boundaries, and batch thickness data export. In the *Normative-Data* publication [36], SAMIRIX used OCTLayerSegmentation by Lang et al. [44], made available by NeuroImaging Tools & Resources Collaboratory (NTRC). This segmentation algorithm was chosen because of its good performance and accuracy with an overall absolute segmentation error of 3.5 µm by combining machine learning and graph-cut algorithms. SAMIRIX was developed out of the need for a reliable pipeline that can be used in day-to-day OCT research. SAMIRIX segments the total macula, mRNFL, GCIPL, INL and several outer retinal layers. Since its introduction, SAMIRIX has been used as the segmentation pipeline in our group and so far used in studies such as the CROCTINO study which has the largest OCT database to date gathered from 501 NMOSD patients from 19 centers worldwide (Annual ECTRIMS Congress 2019, P1300 [45]), a study investigating temporal visual resolution in MS patients [46], and another study describing a retinal phenotype in patients with Spinocerebellar ataxia type 1 [47]. Detailed description of SAMIRIX can be found in the *Normative-Data* publication with an overview of the pipeline and boundaries delineated (Figure 1 of publication [36]) [36]. Figure 1 B (adapted from Figure 1 B of publication [36]) shows a sample B-scan crossing the fovea with the layers studies in the *Normative-Data* study.

Normative data for intraretinal layers

Normative-Data [36]

The normative values for total macular, mRNFL, GCIPL, and INL thicknesses of 423 eyes of 219 healthy volunteers were published in the *Normative-Data* publication [36]. The mean (± SD) for total macular, mRNFL, GCIPL, and INL thicknesses in µm was 313.70 (±12.02), 39.53 (± 3.57), 70.81 (± 4.87), and 35.93 (± 2.34), respectively. Total macular thickness showed an average reduction of 0.21 µm per year ($p = 0.001$), while mRNFL, GCIPL, and INL showed an average reduction of 0.05 ($p = 0.007$), 0.09 ($p = 0.001$), and 0.05 µm ($p < 0.001$) in thickness per year, respectively. Among the four OCT parameters, only total macular and GCIPL thicknesses showed to be significantly thicker in males compared to females (macula: 4.18 µm, ($p = 0.026$), GCIPL: 1.52 µm ($p = 0.029$)). We also analyzed the intercorrelation of GCIPL and INL because of their particular importance in OCT research on CNS autoimmune disorders [25,30]. INL was significantly correlated to GCIPL (correlation coefficient = 0.579 ($p < 0.001$) and showed 0.28 µm increase per 1 µm increase of GCIPL ($p < 0.001$). The mean FT was 281.11 µm (± 19.04). FT showed no significant correlation to age ($p = 0.256$) but was significantly higher in males compared to females (7.77 µm, $p = 0.004$) (see supplementary materials in [36]).

The MDC (and ICC) for total macular, mRNFL, GCIPL, and INL thicknesses for inter-rater reliability was 0.38 (0.99), 0.66 (0.99), 0.46 (0.99), and 0.29 µm (0.99) and for intra-rater reliability was 0.24 (0.99), 0.31 (0.99), 0.23 (0.99), and 0.19 µm (0.99), respectively.

To test the performance of SAMIRIX in comparison to OCT device segmentation (Heidelberg Eye Explorer, HEYEX), 20 OCT scans of NMOSD ON+ eyes were segmented and manually corrected by an experienced grader in both software. NMOSD ON+ eyes were selected because of typically lower quality and thinned layers which are the main cause of segmentation error by different methods. The median for the absolute error of segmentation (the mean absolute correction of all boundaries segmented for total macula, mRNFL, GCIPL, and INL) was 0.16 µm for SAMIRIX and 0.79 µm for HEYEX. The median correction time per eye was 7:59 minutes for SAMIRIX and 10:30 minutes for HEYEX.

A detailed analysis of the normative values are included in the Result section (Table 1-3) [36]. A survey tool to analyze the normative values in different sectors of ETDRS macular map, inter-ocular differences, SAMIRIX performance and more, which allows normative data analysis beyond the scope of the *Normative-Data* manuscript, was written as an interactive HTML document using R Markdown and Shiny packages and was published as supplementary materials of the publication [36].

Foveal shape analysis

Foveal-Shape-Method [37]

A foveal shape analysis method was developed to quantitatively analyze the shape of the fovea. The first step in this method is to flatten OCT images based on the segmentation of BM (reference plane) and then radially reconstruct the ILM surface around the fovea and parafovea up to the maximum points in this area, which are called rim points in this method, using a Cubic Bezier polynomial. Based on the reconstructed ILM surface, 19 parameters are defined that describe the fovea up to the rim points. There are three main surfaces defined by the foveal shape analysis method: 1) Rim Disk that is defined by connecting the rim points, 2) Slope Disk that is defined as a surface connecting the points with maximum slope and characterizes the middle part and width of the fovea, and 3) Pit Flat Disk that lies on the pit of the fovea and describes the flatness of the fovea. Each of these surfaces are described by four parameters: 1) Area, 2) Average Diameter, 3) Major Length, which is defined as the length in the dominant direction or major axis, and 4) Minor Length, which is defined as the length in the second dominant direction or minor axis (perpendicular to the dominant axis). The rest of the parameters are: Inner Rim Volume, defined as the volume between the ILM surface and reference plane in a 1-mm diameter around the center point of the fovea, Rim Volume, defined as the volume between the ILM surface and reference plane within the rim points area, Pit Volume, defined as the volume between the ILM surface and Rim Disk, Average Rim Height, defined as the average height of the rim points, Central Fovea Thickness, defined as the thickness of the thinnest point (the center) of the fovea, Average Pit Depth, defined as the average distance between the minimum points of the fovea

and Rim Disk, and Average Maximum Pit Slope, defined as the average slope of the points with maximum slopes.

The foveal shape analysis method was described in details in the *Foveal-Shape-Method* publication [37]. A short description of the method as well as an overview figure of the parameters was provided in the *NMOSD-Foveal-Shape* publication (Figure 1 in [38]) alongside a consistency assessment for the foveal shape parameters (Supplementary Table e-1 in [38]). Figure 1 C-I (adapted from Figure 1 of publication [38]) shows an overview of the foveal shape analysis method.

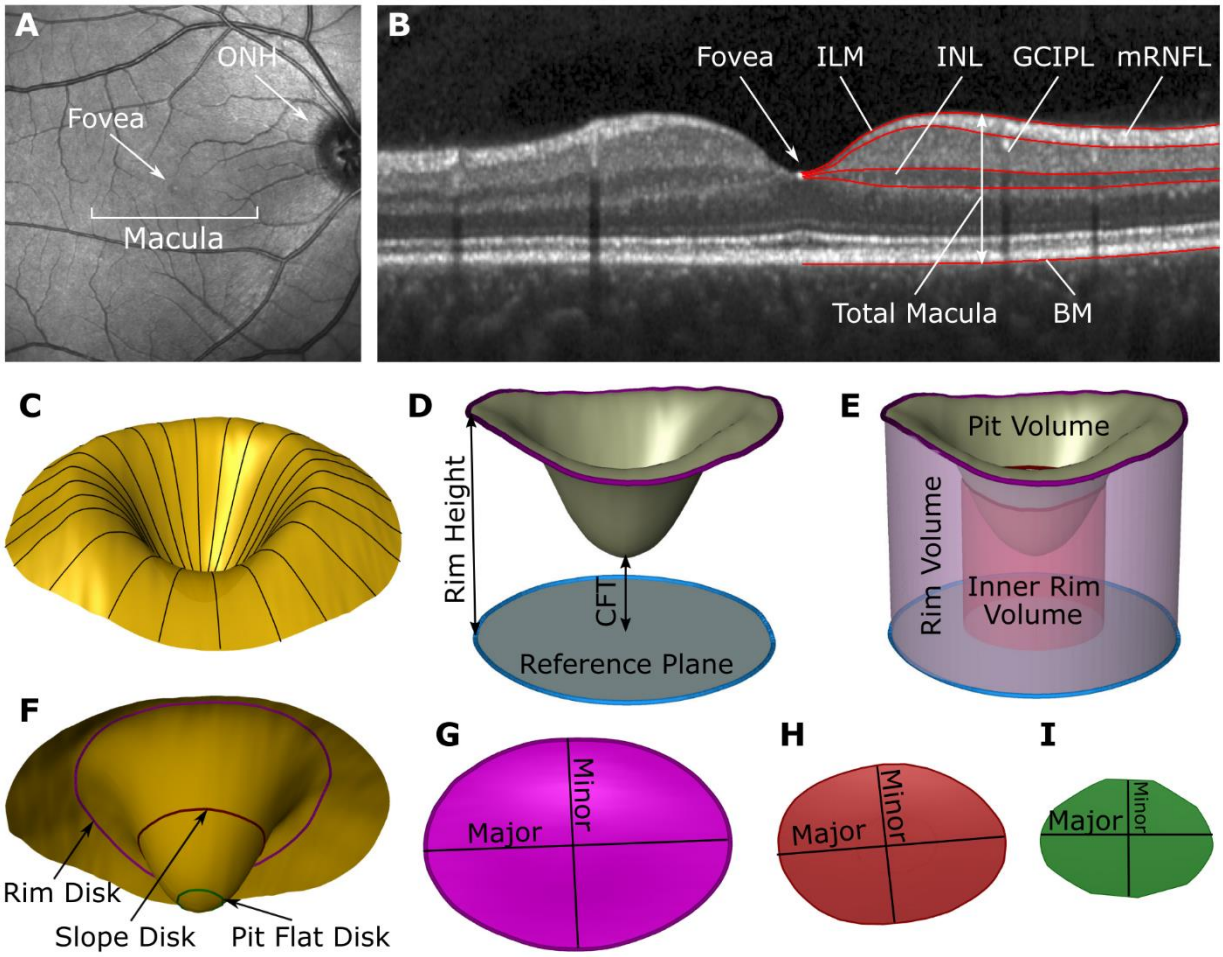

Figure 1: Illustration of retinal layers and foveal shape parameters. (A) A scanning laser ophthalmoscopy image of the retina, (B) a central B-scan crossing the fovea (adapted from Figure 2 B of publication [36]), (C) an example of reconstructed ILM surface by foveal shape analysis method, (D-F) different parameters and surfaces defined by foveal shape analysis method, (G) Rim Disk, (H) Slope Disk, and (I) Pit Flat Disk. C-I was adapted and modified from Figure 1 of publication [38]. Abbreviations: ONH = optic nerve head; ILM = inner limiting membrane; mRNFL = macular retinal nerve fiber layer; GCIPL = combined ganglion cell and inner plexiform layer; INL = inner nuclear layer; BM = Bruch's membrane; CFT = Central Foveal Thickness; Major = major axis; Minor = minor axis.

Foveal shape in NMOSD

NMOSD-Foveal-Shape [38]

First, we compared the foveal shape parameters in NMOSD and MS to HC. The majority of parameters showed significant differences between NMOSD and HC (all 19 parameters except Central Foveal Thickness and Pit Volume) but not between MS and HC (only Average Rim Height, Rim Volume, and Average Maximum Pit Slope out of 19 parameters). This was in contrast to GCIPL and pRNFL, which were significantly lower in both NMOSD and MS patients in comparison to HCs. The detailed results of the comparison is found in Table 2 of the publication [38].

In the next step, we analyzed the power of the foveal shape parameters in discriminating between NMOSD and MS regardless of ON. The parameters describing Pit Flat Disk and Slope Disk plus Inner Rim Volume had AUC above 0.7 in discriminating NMOSD patients from MS patients, where Pit Flat Disk Area had the highest AUC (0.798). The best parameter to discriminate NMOSD from MS among conventional OCT parameters (FT, pRNFL, GCIPL, and INL) was FT with an AUC of 0.66. In addition to the ROC analysis, we looked into the regression analysis of the foveal shape parameters against diagnosis, ON status, and their interaction effect. All the parameters with AUC above 0.7 were shown to be significantly dependent on diagnosis (NMOSD vs. MS) and NMOSD-specific ON but not on the history of ON alone, except for Minor Slope Disk Length, which showed a significant dependency only on diagnosis. We also looked into AUC for distinguishing NMOSD and MS for ON- eyes, to investigate whether the differences seen are at least partially independent of ON-related damage. The best foveal shape parameter to distinguish NMOSD from MS in ON- eyes was Pit Flat Disk Length with an AUC of 0.804, while the best conventional OCT parameter had AUC of 0.691. Of note, pRNFL and GCIPL thicknesses were slightly yet significantly lower in NMOSD ON- eyes compared to HCs (pRNFL: -5.7 µm ($p = 0.017$), GCIPL: -0.12 mm^3 ($p = 0.001$)). Detailed results can be found in Table 3, Supplementary Table e-2 and Figure 2 A-C of the publication [38].

To reduce the number of parameters and select a final set of parameters, we applied a stepwise logistic regression on a linear model predicting NMOSD and MS, based on only the parameters with AUC of greater than 0.7. Stepwise logistic regression selected four parameters: Pit Flat Disk Area, Average Pit Flat Disk Diameter, Inner Rim Volume, and Major Slope Disk Length. These four parameters are displayed in Figure 2 D-E of the publication [38].

The differences observed in foveal shape might be because of more severe retinal damage after ON in NMOSD compared to MS. Hence, we repeated the linear regression analysis with diagnosis, ON status, and their interaction for the selected parameters but this time with correction for either GCIPL or INL. Pit Flat Disk Area, Average Pit Flat Disk Diameter, and Inner Rim Volume showed a significant association to diagnosis, NMOSD-specific ON, and GCIPL (when corrected for GCIPL) but not ON and INL (when corrected for INL). Major Slope Disk Length showed a significant relationship only with NMOSD-specific ON. Detailed analysis is found in Table 4 and Supplementary Table e-3 of the publication [38].

Finally, we looked into foveal shape in a second independent cohort of NMOSD and MS patients, in order to test whether similar changes could be seen. In a repeated regression analysis on the

selected parameters in the confirmatory cohort against diagnosis, ON, and their interaction, Pit Flat Disk Area and Average Pit Flat Disk Diameter were shown to be significantly dependent on diagnosis but neither on ON nor on NMOSD-specific ON. Major Slope Disk Length showed significant correlation only with NMOSD-specific ON and Inner Rim Volume showed no significant differences between groups.

Discussion

In this work, I aimed to improve the image analysis of macular OCT images by 1) introducing a new segmentation pipeline and presenting normative data for inner retinal layers in a large dataset of 423 eyes of 218 healthy volunteers [36], and 2) introducing a novel foveal shape analysis method [37] and investigating foveal shape alteration in AQP4-IgG-seropositive patients regardless of ON status [38].

In the *Normative-Data* study, we showed significant thinning in thicknesses of macula, mRNFL, GCIPL, and INL in healthy controls over age. This finding is in line with other studies such as a study by Invernizzi et al. [48] who showed different intraretinal layers thinning in the outer and middle rings of the ETDRS macular map but not in the center sector (the fovea), based on macula scans from Spectralis SD-OCT. We also showed a thinner macula and GCIPL in women compared to men, and no significant differences in mRNFL and INL. Most studies, like Song et al. [49], showed thinner intraretinal layers in women compared to men, which is in line with our findings for macula and GCIPL but not for mRNFL and INL. Inter-rater and intra-rater reliability was excellent (ICC values above 0.99) for manual correction of segmentation boundaries. The MDC reported for inter-rater reliability is higher than the projected annual loss for instance in GCIPL in MS patients (−1.1 µm over 2 years [50]), but is still lower than the resolution of current OCT technology, which indicates that imaging and not segmentation is the limiting parameter in retinal OCT research. This emphasizes the need for more sensitive image analysis tools for OCT images in order to detect small but relevant changes in patients. We also investigated the relationship of GCIPL and INL in healthy controls. Our analysis showed significant positive correlations between the thicknesses of GCIPL and INL, which can be used as a reference in studies looking into GCIPL and INL in neuroinflammatory diseases, where these two layers sometimes go in opposite directions with GCIPL thickness showing reduction because of neurodegeneration [24] and INL showing thickening due to inflammation [29].

The introduced semi-automatic segmentation toolbox (SAMIRIX) offers a wide variety of tools for the entire process of retinal image analysis for Spectralis SD-OCT images. While SAMIRIX uses a third-party segmentation algorithm, it provides customized preprocessing, post-processing, and segmentation review and correction tools, which facilitate retinal OCT research. In comparison to the device-specific segmentation tool HEYEX, SAMIRIX was shown to be more accurate in segmentation and faster for manual correction. Another advantage of SAMIRIX is its accessibility for research as an open-source pipeline, which gets updated regularly to offer more options, such

as a recently added option of segmenting OCT images from different devices, which optimizes pooling of data from different devices.

While we report normative data in a large dataset and provide a survey tool for detailed analysis of the data, this study is limited to one device and one scanning protocol, which limits generalizability. Additionally, the study included only OCT scans from people with Caucasian ethnicity and thus the findings are not necessarily extendable to other ethnicities, as studies showed differences in intraretinal layer thicknesses in different ethnic groups, such as Grover et al. [51], who showed thicker retina in Black subjects compared to Caucasian subjects.

In the *Foveal-Shape-Method* study, we introduced a robust and accurate method for foveal shape analysis that provides a quantitative characterization of the fovea. The method allows us to investigate foveal changes based on retinal OCT images in patients with autoimmune neuroinflammatory diseases of CNS, beyond the conventional use of intraretinal thicknesses and volumes [37]. The proposed method compared to other foveal shape analysis approaches [52,53] is simpler and more robust thanks to the intuitive interpretation of the parameters due to the direct relation of the parameters to geometry, which greatly improves its potential applications in the medical field. Another advantage of the foveal shape analysis method is its ability to describe the foveal region from the 3D and not 2D cross-sectional perspective, which enables the researcher/clinician to capture more relevant details.

In the *NMOSD-Foveal-Shape* study of this work [38], we showed wider and flatter fovea in AQP4-IgG-seropositive NMOSD compared to HC and MS, characterized by increased Pit Flat Disk Area, Average Pit Flat Disk Diameter, Major Slope Disk Length, and reduced Inner Rim Volume. The observed changes in foveal shape were in ON+ and ON- eyes and were still present when we corrected for ON and neuro-axonal damage in statistical models, indicative of an alteration in the fovea beyond neuro-axonal damage caused by ON. The findings of this study further detail previous findings by Jeong et al. [31] and later in our own study by Oertel and Kuchling et al. [32], who showed thinning in FT in AQP4-IgG-seropositive NMOSD independent of ON in comparison to HC, which is an indirect evidence of foveal shape alteration.

A pathological cause for the observed foveal shape changes could be an AQP4-IgG-mediated primary retinopathy in AQP4-IgG-seropositive NMOSD. Müller cells, the principal glial cells in the retina, which span the entire thickness of the retina and are densely present around the fovea, express AQP4 and might be damaged by AQP4-IgG. This hypothesis is supported by animal studies that showed AQP4-IgG induced AQP4 loss in Müller cells in rats [33,34]. Autopsy cases in AQP4-IgG-seropositive NMOSD also suggested complement-independent AQP4-IgG mediated Müller cell damage in human [35]. For AQP4-IgG to reach Müller cells in the retina, the blood-retinal- or blood-brain-barrier has to be disrupted [54], which is often the case acute inflammatory events. Yet the question needs to be answered whether the blood-retinal- or blood-brain-barrier is disrupted in NMOSD without fully activating complement cascades. A recent study

on rats has shown that circulating AQP4-IgG in cerebrospinal fluid can cause NMOSD, indicative of complement independent damage without blood-brain-barrier breakdown [55].

Another possible pathophysiological cause of foveal changes could be subclinical ON, as studies have shown neuro-axonal damage in ON- eyes of AQP4-IgG-seropositive NMOSD patients [56]. Another possible reason for the observed changes in the fovea could be the chiasmal crossover of neuro-axonal damage from ON-affected eyes to their non-affected fellow eyes, as ON in AQP4-IgG-seropositive patients often involves the chiasm, contrary to MS [10,57]. Significant differences in pRNFL and GCIPL thicknesses in NMOSD ON- eyes compared to HC are supportive of these two hypotheses.

In this study, we were not able to investigate cross-chiasmal effects due to an insufficient number of NMOSD patients included who had never experienced ON. Although we ruled out potential errors stemming from protocol or device bias by only including macular OCT scans from one device scanned with a single scanning protocol, this prevented us from evaluating the impacts of using different devices and scan protocols on the foveal shape parameters and results. Multi-device and multi-center validations are still required.

Foveal shape analysis may improve the differential diagnosis of AQP4-IgG-seropositive NMOSD and promote the use of OCT as diagnostic tool. The need for improved differential diagnostic tools highlighted by the fact that the use of MS therapeutic approaches in NMOSD patients that are misdiagnosed and treated as MS can be ineffective or even cause disease worsening [58]. The four selected foveal shape parameters show significant differences in NMOSD compared to MS regardless of ON, whereas conventional OCT parameters, such as pRNFL and GCIPL, mostly show significant dependency on ON. From the four selected parameters, only Pit Flat Disk Area and Average Pit Flat Disk Diameter were confirmed in a second cohort. A possible reason for this inconsistency in the confirmatory cohort could be the significant difference in ON frequency between NMOSD and MS patients in the cohort, which indicates the need for further confirmation. Future work should investigate longitudinal changes of the foveal shape parameters in AQP4-IgG-seropositive NMOSD patients, foveal shape differences in subtypes of NMOSD, and foveal shape parameters dependency on scan protocols and OCT devices.

In conclusion, the outcomes of this work could help us getting closer to establish retinal OCT as a standard imaging modality in clinical routines of MS and NMOSD. SAMIRIX is a robust segmentation pipeline and the here presented normative data and minimally detectable changes will aid in interpreting data from neurodegenerative and neuroinflammatory disorders. The foveal shape analysis method and the shown foveal shape changes in AQP4-IgG-seropositive NMOSD in comparison to MS and HC would potentially lead to higher specificity and sensitivity in diagnosis, enhanced disease progression monitoring, better understanding of underlying disease mechanisms, and improved therapeutic strategies for NMOSD, MS, and other autoimmune disorders of the CNS.

References

[1] Reich, D.S.; Lucchinetti, C.F.; Calabresi, P.A. Multiple Sclerosis. *N Engl J Med*, **2018**, *378*, 169–180.

[2] Krieger, S.C.; Cook, K.; De Nino, S.; Fletcher, M. The Topographical Model of Multiple Sclerosis: A Dynamic Visualization of Disease Course. *Neurol Neuroimmunol Neuroinflamm*, **2016**, *3*, e279.

[3] Jarius, S.; Wildemann, B.; Paul, F. Neuromyelitis Optica: Clinical Features, Immunopathogenesis and Treatment: Neuromyelitis Optica. *Clin Exp Immunol*, **2014**, *176*, 149–164.

[4] Zekeridou, A.; Lennon, V.A. Aquaporin-4 Autoimmunity. *Neurol Neuroimmunol Neuroinflamm*, **2015**, *2*, e110.

[5] Paul, F.; Jarius, S.; Aktas, O.; Bluthner, M.; Bauer, O.; Appelhans, H.; Franciotta, D.; Bergamaschi, R.; Littleton, E.; Palace, J.; Seelig, H.-P.; Hohlfeld, R.; Vincent, A.; Zipp, F. Antibody to Aquaporin 4 in the Diagnosis of Neuromyelitis Optica. *PLoS Med*, **2007**, *4*, e133.

[6] Jarius, S.; Ruprecht, K.; Wildemann, B.; Kuempfel, T.; Ringelstein, M.; Geis, C.; Kleiter, I.; Kleinschnitz, C.; Berthele, A.; Brettschneider, J.; Hellwig, K.; Hemmer, B.; Linker, R.A.; Lauda, F.; Mayer, C.A.; Tumani, H.; Melms, A.; Trebst, C.; Stangel, M.; Marziniak, M.; Hoffmann, F.; Schippling, S.; Faiss, J.H.; Neuhaus, O.; Ettrich, B.; Zentner, C.; Guthke, K.; Hofstadt-van Oy, U.; Reuss, R.; Pellkofer, H.; Ziemann, U.; Kern, P.; Wandinger, K.P.; Then Bergh, F.; Boettcher, T.; Langel, S.; Liebetrau, M.; Rommer, P.S.; Niehaus, S.; Münch, C.; Winkelmann, A.; Zettl U, U.K.; Metz, I.; Veauthier, C.; Sieb, J.P.; Wilke, C.; Hartung, H.P.; Aktas, O.; Paul, F. Contrasting Disease Patterns in Seropositive and Seronegative Neuromyelitis Optica: A Multicentre Study of 175 Patients. *J Neuroinflammation*, **2012**, *9*, 503.

[7] Papadopoulos, M.C.; Bennett, J.L.; Verkman, A.S. Treatment of Neuromyelitis Optica: State-of-the-Art and Emerging Therapies. *Nat Rev Neurol*, **2014**, *10*, 493–506.

[8] Hinson, S.R.; Romero, M.F.; Popescu, B.F.G.; Lucchinetti, C.F.; Fryer, J.P.; Wolburg, H.; Fallier-Becker, P.; Noell, S.; Lennon, V.A. Molecular Outcomes of Neuromyelitis Optica (NMO)-IgG Binding to Aquaporin-4 in Astrocytes. *Proceedings of the National Academy of Sciences*, **2012**, *109*, 1245–1250.

[9] Toosy, A.T.; Mason, D.F.; Miller, D.H. Optic Neuritis. *The Lancet Neurology*, **2014**, *13*, 83–99.

[10] Ramanathan, S.; Prelog, K.; Barnes, E.H.; Tantsis, E.M.; Reddel, S.W.; Henderson, A.P.; Vucic, S.; Gorman, M.P.; Benson, L.A.; Alper, G.; Riney, C.J.; Barnett, M.; Parratt, J.D.; Hardy, T.A.; Leventer, R.J.; Merheb, V.; Nosadini, M.; Fung, V.S.; Brilot, F.; Dale, R.C. Radiological Differentiation of Optic Neuritis with Myelin Oligodendrocyte Glycoprotein Antibodies, Aquaporin-4 Antibodies, and Multiple Sclerosis. *Mult Scler*, **2016**, *22*, 470–482.

[11] Bennett, J.; de Seze, J.; Lana-Peixoto, M.; Palace, J.; Waldman, A.; Schippling, S.; Tenembaum, S.; Banwell, B.; Greenberg, B.; Levy, M.; Fujihara, K.; Chan, K.; Kim, H.; Asgari, N.; Sato, D.; Saiz, A.; Wuerfel, J.; Zimmermann, H.; Green, A.; Villoslada, P.; Paul, F.; with the GJCF-ICC&BR. Neuromyelitis Optica and Multiple Sclerosis: Seeing Differences through Optical Coherence Tomography. *Mult Scler*, **2015**, *21*, 678–688.

[12] Oertel, F.C.; Zimmermann, H.; Paul, F.; Brandt, A.U. Optical Coherence Tomography in Neuromyelitis Optica Spectrum Disorders: Potential Advantages for Individualized Monitoring of Progression and Therapy. *EPMA Journal*, **2018**, *9*, 21–33.

[13] MacKay, D.D.; Galetta, S.L.; Prasad, S. Anatomy of the Anterior Visual Pathway. In *Optical Coherence Tomography in Neurologic Diseases*; Calabresi, P.A.; Balcer, L.J.; Frohman, E.M., Eds.; Cambridge University Press: Cambridge, **2015**; pp. 14–27.

[14] Bringmann, A.; Pannicke, T.; Grosche, J.; Francke, M.; Wiedemann, P.; Skatchkov, S.; Osborne, N.; Reichenbach, A. Müller Cells in the Healthy and Diseased Retina. *Progress in Retinal and Eye Research*, **2006**, *25*, 397–424.

[15] Helga Kolb, E.F., and Ralph Nelson [editors]. *Webvision : The Organization of the Retina and Visual System*; [Bethesda, Md.] : National Library of Medicine : [National Center for Biotechnology Information], 2007., **2007**.

[16] Hrynchak, P.; Simpson, T. Optical Coherence Tomography: An Introduction to the Technique and Its Use: *Optometry and Vision Science*, **2000**, *77*, 347–356.

[17] Brandt, A.U.; Martinez-Lapiscina, E.H.; Nolan, R.; Saidha, S. Monitoring the Course of MS With Optical Coherence Tomography. *Curr Treat Options Neurol*, **2017**, *19*, 15.

[18] Tewarie, P.; Balk, L.; Costello, F.; Green, A.; Martin, R.; Schippling, S.; Petzold, A. The OSCAR-IB Consensus Criteria for Retinal OCT Quality Assessment. *PLoS ONE*, **2012**, *7*, e34823.

[19] Cruz-Herranz, A.; Balk, L.J.; Oberwahrenbrock, T.; Saidha, S.; Martinez-Lapiscina, E.H.; Lagreze, W.A.; Schuman, J.S.; Villoslada, P.; Calabresi, P.; Balcer, L.; Petzold, A.; Green, A.J.; Paul, F.; Brandt, A.U.; Albrecht, P. The APOSTEL Recommendations for Reporting Quantitative Optical Coherence Tomography Studies. *Neurology*, **2016**, *86*, 2303–2309.

[20] Schneider, E.; Zimmermann, H.; Oberwahrenbrock, T.; Kaufhold, F.; Kadas, E.M.; Petzold, A.; Bilger, F.; Borisow, N.; Jarius, S.; Wildemann, B.; Ruprecht, K.; Brandt, A.U.; Paul, F. Optical Coherence Tomography Reveals Distinct Patterns of Retinal Damage in Neuromyelitis Optica and Multiple Sclerosis. *PLoS ONE*, **2013**, *8*, e66151.

[21] Petzold, A.; Wattjes, M.P.; Costello, F.; Flores-Rivera, J.; Fraser, C.L.; Fujihara, K.; Leavitt, J.; Marignier, R.; Paul, F.; Schippling, S.; Sindic, C.; Villoslada, P.; Weinshenker, B.; Plant, G.T. The Investigation of Acute Optic Neuritis: A Review and Proposed Protocol. *Nat Rev Neurol*, **2014**, *10*, 447–458.

[22] Oertel, F.C.; Zimmermann, H.; Mikolajczak, J.; Weinhold, M.; Kadas, E.M.; Oberwahrenbrock, T.; Pache, F.; Bellmann-Strobl, J.; Ruprecht, K.; Paul, F.; Brandt, A.U. Contribution of Blood Vessels to Retinal Nerve Fiber Layer Thickness in NMOSD. *Neurol Neuroimmunol Neuroinflamm*, **2017**, *4*, e338.

[23] Oberwahrenbrock, T.; Traber, G.L.; Lukas, S.; Gabilondo, I.; Nolan, R.; Songster, C.; Balk, L.; Petzold, A.; Paul, F.; Villoslada, P.; Brandt, A.U.; Green, A.J.; Schippling, S. Multicenter Reliability of Semiautomatic Retinal Layer Segmentation Using OCT. *Neurol Neuroimmunol Neuroinflamm*, **2018**, *5*, e449.

[24] Petzold, A.; Balcer, L.J.; Calabresi, P.A.; Costello, F.; Frohman, T.C.; Frohman, E.M.; Martinez-Lapiscina, E.H.; Green, A.J.; Kardon, R.; Outteryck, O.; Paul, F.; Schippling, S.; Vermersch, P.; Villoslada, P.; Balk, L.J.; Aktas, O.; Albrecht, P.; Ashworth, J.; Asgari, N.; Balcer, L.; Balk, L.; Black, G.; Boehringer, D.; Behbehani, R.; Benson, L.; Bermel, R.; Bernard, J.; Brandt, A.; Burton, J.; Calabresi, P.; Calkwood, J.; Cordano, C.; Costello, F.; Courtney, A.; Cruz-Herranz, A.; Diem, R.; Daly, A.; Dollfus, H.; Fasser, C.; Finke, C.; Frederiksen, J.; Frohman, E.; Frohman, T.; Garcia-Martin, E.; Suárez, I.G.; Pihl-Jensen, G.; Graves, J.; Green, A.; Havla, J.; Hemmer, B.; Huang, S.-C.; Imitola, J.; Jiang, H.; Keegan, D.; Kildebeck, E.; Klistorner, A.; Knier, B.; Kolbe, S.; Korn, T.; LeRoy, B.; Leocani, L.; Leroux, D.; Levin, N.; Liskova, P.; Lorenz, B.; Preiningerova, J.L.; Martínez-Lapiscina, E.H.; Mikolajczak, J.; Montalban, X.; Morrow, M.; Nolan, R.; Oberwahrenbrock, T.; Oertel, F.C.; Oreja-Guevara, C.; Osborne, B.; Outteryck, O.; Papadopoulou, A.; Paul, F.; Petzold, A.; Ringelstein, M.; Saidha, S.; Sanchez-Dalmau, B.; Sastre-Garriga, J.; Schippling, S.; Shin, R.; Shuey, N.; Soelberg, K.; Toosy, A.; Torres, R.; Vidal-Jordana, A.; Villoslada, P.; Waldman, A.; White, O.; Yeh, A.; Wong, S.; Zimmermann, H. Retinal Layer Segmentation in Multiple Sclerosis: A Systematic Review and Meta-Analysis. *The Lancet Neurology*, **2017**, *16*, 797–812.

[25] Syc, S.B.; Saidha, S.; Newsome, S.D.; Ratchford, J.N.; Levy, M.; Ford, E.; Crainiceanu, C.M.; Durbin, M.K.; Oakley, J.D.; Meyer, S.A.; Frohman, E.M.; Calabresi, P.A. Optical Coherence Tomography Segmentation Reveals Ganglion Cell Layer Pathology after Optic Neuritis. *Brain*, **2012**, *135*, 521–533.

[26] Martinez-Lapiscina, E.H.; Arnow, S.; Wilson, J.A.; Saidha, S.; Preiningerova, J.L.; Oberwahrenbrock, T.; Brandt, A.U.; Pablo, L.E.; Guerrieri, S.; Gonzalez, I.; Outteryck, O.; Mueller, A.-K.; Albrecht, P.; Chan, W.; Lukas, S.; Balk, L.J.; Fraser, C.; Frederiksen, J.L.; Resto, J.; Frohman, T.; Cordano, C.; Zubizarreta, I.; Andorra, M.; Sanchez-Dalmau, B.; Saiz, A.; Bermel, R.; Klistorner, A.; Petzold, A.; Schippling, S.; Costello, F.; Aktas, O.; Vermersch, P.; Oreja-Guevara, C.; Comi, G.; Leocani, L.; Garcia-Martin, E.; Paul, F.; Havrdova, E.; Frohman, E.; Balcer, L.J.; Green, A.J.; Calabresi, P.A.; Villoslada, P. Retinal Thickness Measured with Optical Coherence Tomography and Risk of Disability Worsening in Multiple Sclerosis: A Cohort Study. *The Lancet Neurology*, **2016**, *15*, 574–584.

[27] Zimmermann, H.G.; Knier, B.; Oberwahrenbrock, T.; Behrens, J.; Pfuhl, C.; Aly, L.; Kaminski, M.; Hoshi, M.-M.; Specovius, S.; Giess, R.M.; Scheel, M.; Mühlau, M.; Bellmann-Strobl, J.; Ruprecht, K.; Hemmer, B.; Korn, T.; Paul, F.; Brandt, A.U. Association of Retinal Ganglion Cell Layer Thickness With Future Disease Activity in Patients With Clinically Isolated Syndrome. *JAMA Neurol*, **2018**, *75*, 1071.

[28] Kaufhold, F.; Zimmermann, H.; Schneider, E.; Ruprecht, K.; Paul, F.; Oberwahrenbrock, T.; Brandt, A.U. Optic Neuritis Is Associated with Inner Nuclear Layer Thickening and Microcystic Macular Edema Independently of Multiple Sclerosis. *PLoS ONE*, **2013**, *8*, e71145.

[29] Knier, B.; Schmidt, P.; Aly, L.; Buck, D.; Berthele, A.; Mühlau, M.; Zimmer, C.; Hemmer, B.; Korn, T. Retinal Inner Nuclear Layer Volume Reflects Response to Immunotherapy in Multiple Sclerosis. *Brain*, **2016**, *139*, 2855–2863.

[30] Balk, L.J.; Coric, D.; Knier, B.; Zimmermann, H.G.; Behbehani, R.; Alroughani, R.; Martinez-Lapiscina, E.H.; Brandt, A.U.; Sánchez-Dalmau, B.; Vidal-Jordana, A.; Albrecht, P.; Koska, V.; Havla, J.; Pisa, M.; Nolan, R.C.; Leocani, L.; Paul, F.; Aktas, O.; Montalban, X.; Balcer, L.J.; Villoslada, P.; Outteryck, O.; Korn, T.; Petzold, A.; on behalf of the IMSVISUAL consortium. Retinal Inner Nuclear Layer Volume Reflects Inflammatory Disease Activity in Multiple Sclerosis; a Longitudinal OCT Study. *Multiple Sclerosis Journal - Experimental, Translational and Clinical*, **2019**, *5*, 205521731987158.

[31] Jeong, I.H.; Kim, H.J.; Kim, N.-H.; Jeong, K.S.; Park, C.Y. Subclinical Primary Retinal Pathology in Neuromyelitis Optica Spectrum Disorder. *J Neurol*, **2016**, *263*, 1343–1348.

[32] Oertel, F.C.; Kuchling, J.; Zimmermann, H.; Chien, C.; Schmidt, F.; Knier, B.; Bellmann-Strobl, J.; Korn, T.; Scheel, M.; Klistorner, A.; Ruprecht, K.; Paul, F.; Brandt, A.U. Microstructural Visual System Changes in AQP4-Antibody–Seropositive NMOSD. *Neurol Neuroimmunol Neuroinflamm*, **2017**, *4*, e334.

[33] Felix, C.M.; Levin, M.H.; Verkman, A.S. Complement-Independent Retinal Pathology Produced by Intravitreal Injection of Neuromyelitis Optica Immunoglobulin G. *J Neuroinflammation*, **2016**, *13*, 275.

[34] Zeka, B.; Hastermann, M.; Kaufmann, N.; Schanda, K.; Pende, M.; Misu, T.; Rommer, P.; Fujihara, K.; Nakashima, I.; Dahle, C.; Leutmezer, F.; Reindl, M.; Lassmann, H.; Bradl, M. Aquaporin 4-Specific T Cells and NMO-IgG Cause Primary Retinal Damage in Experimental NMO/SD. *acta neuropathol commun*, **2016**, *4*, 82.

[35] Hokari, M.; Yokoseki, A.; Arakawa, M.; Saji, E.; Yanagawa, K.; Yanagimura, F.; Toyoshima, Y.; Okamoto, K.; Ueki, S.; Hatase, T.; Ohashi, R.; Fukuchi, T.; Akazawa, K.; Yamada, M.; Kakita, A.; Takahashi, H.; Nishizawa, M.; Kawachi, I. Clinicopathological Features in Anterior Visual Pathway in Neuromyelitis Optica. *Ann. Neurol.*, **2016**, *79*, 605–624.

[36] Motamedi, S.; Gawlik, K.; Ayadi, N.; Zimmermann, H.G.; Asseyer, S.; Bereuter, C.; Mikolajczak, J.; Paul, F.; Kadas, E.M.; Brandt, A.U. Normative Data and Minimally Detectable Change for Inner Retinal Layer Thicknesses Using a Semi-Automated OCT Image Segmentation Pipeline. *Front. Neurol.*, **2019**, *10*, 1117.

[37] Yadav, S.K.; Motamedi, S.; Oberwahrenbrock, T.; Oertel, F.C.; Polthier, K.; Paul, F.; Kadas, E.M.; Brandt, A.U. CuBe: Parametric Modeling of 3D Foveal Shape Using Cubic Bézier. *Biomed. Opt. Express*, **2017**, *8*, 4181.

[38] Motamedi, S.; Oertel, F.C.; Yadav, S.K.; Kadas, E.M.; Weise, M.; Havla, J.; Ringelstein, M.; Aktas, O.; Albrecht, P.; Ruprecht, K.; Bellmann-Strobl, J.; Zimmermann, H.G.; Paul, F.; Brandt, A.U. Altered Fovea in AQP4-IgG–Seropositive Neuromyelitis Optica Spectrum Disorders. *Neurol Neuroimmunol Neuroinflamm*, **2020**, *7*, e805.

[39] Wingerchuk, D.M.; Banwell, B.; Bennett, J.L.; Cabre, P.; Carroll, W.; Chitnis, T.; de Seze, J.; Fujihara, K.; Greenberg, B.; Jacob, A.; Jarius, S.; Lana-Peixoto, M.; Levy, M.; Simon, J.H.; Tenembaum, S.; Traboulsee, A.L.; Waters, P.; Wellik, K.E.; Weinshenker, B.G. International Consensus Diagnostic Criteria for Neuromyelitis Optica Spectrum Disorders. *Neurology*, **2015**, *85*, 177–189.

[40] Huang, D.; Swanson, E.A.; Lin, C.P.; Schuman, J.S.; Stinson, W.G.; Chang, W.; Hee, M.R.; Flotte, T.; Gregory, K.; Puliafito, C.A. Optical Coherence Tomography. *Science*, **1991**, *254*, 1178–1181.

[41] de Boer, J.F.; Leitgeb, R.; Wojtkowski, M. Twenty-Five Years of Optical Coherence Tomography: The Paradigm Shift in Sensitivity and Speed Provided by Fourier Domain OCT [Invited]. *Biomed. Opt. Express*, **2017**, *8*, 3248.

[42] ETDRS Research Group. Grading Diabetic Retinopathy from Stereoscopic Color Fundus Photographs–an Extension of the Modified Airlie House Classification. ETDRS Report Number 10. Early Treatment Diabetic Retinopathy Study Research Group. *Ophthalmology*, **1991**, *98*, 786–806.

[43] Beckerman, H.; Roebroeck, M.E.; Lankhorst, G.J.; Becher, J.G.; Bezemer, P.D.; Verbeek, A.L.M. Smallest Real Difference, a Link between Reproducibility and Responsiveness. *Quality of Life Research*, **2001**, *10*, 571–578.

[44] Lang, A.; Carass, A.; Hauser, M.; Sotirchos, E.S.; Calabresi, P.A.; Ying, H.S.; Prince, J.L. Retinal Layer Segmentation of Macular OCT Images Using Boundary Classification. *Biomed. Opt. Express*, **2013**, *4*, 1133.

[45] Oertel, F.C.; Specovius, S.; Zimmermann, H.G.; Chien, C.; Motamedi, S.; Cook, L.; Martinez-Lapiscina, E.H.; Lana Peixoto, M.A.; Fontenelle, M.A.; Palace, J.; Roca-Fernandez, A.; Siritho, S.; Altintas, A.; Tanriverdi, U.; Jacob, A.; Huda, S.; Marignier, R.; Nerrant, E.; Cobo Calvo, A.; de Sèze, J.; Senger, T.; Pandit, L.; Dcunha, A.; de Castillo, I.S.; Bichuetti, D.; Tavares, M.; May,

E.F.; Tongco, C.; Havla, J.; Leocani, L.; Pisa, M.; Ashtari, F.; Kafieh, R.; Aktas, O.; Ringelstein, M.; Albrecht, P.; Kim, H.J.; Hyun, J.-W.; Asgari, N.; Soelberg, K.; Mao-Draayer, Y.; Stiebel-Kalish, H.; Rimler, Z.; Reid, A.; Yeaman, M.; Smith, T.J.; Brandt, A.U.; Paul, F.; GJCF International Clinical Consortium for NMOSD. ECTRIMS 2019 - Poster Session 3 - P1300 - An International Retrospective Multi-Center Study of Retinal Optical Coherence Tomography in Neuromyelitis Optica Spectrum Disorders: The CROCTINO Study. *Mult Scler*, **2019**, *25*, 581–805.

[46] Ayadi, N.; Dörr, J.; Motamedi, S.; Gawlik, K.; Bellmann-Strobl, J.; Mikolajczak, J.; Brandt, A.U.; Zimmermann, H.; Paul, F. Temporal Visual Resolution and Disease Severity in MS. *Neurol Neuroimmunol Neuroinflamm*, **2018**, *5*, e492.

[47] Oertel, F.C.; Zeitz, O.; Rönnefarth, M.; Bereuter, C.; Motamedi, S.; Zimmermann, H.G.; Kuchling, J.; Grosch, A.S.; Doss, S.; Browne, A.; Paul, F.; Schmitz-Hübsch, T.; Brandt, A.U. Functionally Relevant Maculopathy and Optic Atrophy in Spinocerebellar Ataxia Type 1. *Mov Disord Clin Pract*, **2020**, mdc3.12949.

[48] Invernizzi, A.; Pellegrini, M.; Acquistapace, A.; Benatti, E.; Erba, S.; Cozzi, M.; Cigada, M.; Viola, F.; Gillies, M.; Staurenghi, G. Normative Data for Retinal-Layer Thickness Maps Generated by Spectral-Domain OCT in a White Population. *Ophthalmology Retina*, **2018**, *2*, 808-815.e1.

[49] Song, W.K.; Lee, S.C.; Lee, E.S.; Kim, C.Y.; Kim, S.S. Macular Thickness Variations with Sex, Age, and Axial Length in Healthy Subjects: A Spectral Domain–Optical Coherence Tomography Study. *Invest. Ophthalmol. Vis. Sci.*, **2010**, *51*, 3913.

[50] Balk, L.J.; Cruz-Herranz, A.; Albrecht, P.; Arnow, S.; Gelfand, J.M.; Tewarie, P.; Killestein, J.; Uitdehaag, B.M.J.; Petzold, A.; Green, A.J. Timing of Retinal Neuronal and Axonal Loss in MS: A Longitudinal OCT Study. *J Neurol*, **2016**, *263*, 1323–1331.

[51] Grover, S.; Murthy, R.K.; Brar, V.S.; Chalam, K.V. Normative Data for Macular Thickness by High-Definition Spectral-Domain Optical Coherence Tomography (Spectralis). *American Journal of Ophthalmology*, **2009**, *148*, 266–271.

[52] Ding, Y.; Spund, B.; Glazman, S.; Shrier, E.M.; Miri, S.; Selesnick, I.; Bodis-Wollner, I. Application of an OCT Data-Based Mathematical Model of the Foveal Pit in Parkinson Disease. *J Neural Transm*, **2014**, *121*, 1367–1376.

[53] Scheibe, P.; Lazareva, A.; Braumann, U.-D.; Reichenbach, A.; Wiedemann, P.; Francke, M.; Rauscher, F.G. Parametric Model for the 3D Reconstruction of Individual Fovea Shape from OCT Data. *Experimental Eye Research*, **2014**, *119*, 19–26.

[54] Takeshita, Y.; Obermeier, B.; Cotleur, A.C.; Spampinato, S.F.; Shimizu, F.; Yamamoto, E.; Sano, Y.; Kryzer, T.J.; Lennon, V.A.; Kanda, T.; Ransohoff, R.M. Effects of Neuromyelitis Optica–IgG at the Blood–Brain Barrier in Vitro. *Neurol Neuroimmunol Neuroinflamm*, **2017**, *4*, e311.

[55] Hillebrand, S.; Schanda, K.; Nigritinou, M.; Tsymala, I.; Böhm, D.; Peschl, P.; Takai, Y.; Fujihara, K.; Nakashima, I.; Misu, T.; Reindl, M.; Lassmann, H.; Bradl, M. Circulating AQP4-Specific Auto-Antibodies Alone Can Induce Neuromyelitis Optica Spectrum Disorder in the Rat. *Acta Neuropathol*, **2019**, *137*, 467–485.

[56] Ringelstein, M.; Harmel, J.; Zimmermann, H.; Brandt, A.U.; Paul, F.; Haarmann, A.; Buttmann, M.; Hümmert, M.W.; Trebst, C.; Schroeder, C.; Ayzenberg, I.; Kleiter, I.; Hellwig, K.; Havla, J.; Kümpfel, T.; Jarius, S.; Wildemann, B.; Rommer, P.; Weber, M.S.; Pellkofer, H.; Röpke, L.; Geis, C.; Retzlaff, N.; Zettl, U.; Deppe, M.; Klotz, L.; Young, K.; Stellmann, J.-P.; Kaste, M.; Kermer, P.; Marouf, W.; Lauda, F.; Tumani, H.; Graf, J.; Klistorner, A.; Hartung, H.-P.; Aktas, O.; Albrecht, P.; on behalf of the Neuromyelitis Optica Study Group (NEMOS). Longitudinal Optic Neuritis-Unrelated Visual Evoked Potential Changes in NMO Spectrum Disorders. *Neurology*, **2020**, *94*, e407–e418.

[57] Juenger, V.; Cooper, G.; Chien, C.; Chikermane, M.; Oertel, F.C.; Zimmermann, H.; Ruprecht, K.; Jarius, S.; Siebert, N.; Kuchling, J.; Papadopoulou, A.; Asseyer, S.; Bellmann-Strobl, J.; Paul, F.; Brandt, A.U.; Scheel, M. Optic Chiasm Measurements May Be Useful Markers of Anterior Optic Pathway Degeneration in Neuromyelitis Optica Spectrum Disorders. *Eur Radiol*, **2020**.

[58] Kleiter, I.; Hellwig, K.; Berthele, A.; Kümpfel, T.; Linker, R.A.; Hartung, H.-P.; Paul, F.; Aktas, O.; for the Neuromyelitis Optica Study Group. Failure of Natalizumab to Prevent Relapses in Neuromyelitis Optica. *Arch Neurol*, **2012**, *69*, 239.

Statutory Declaration

“I, Seyedamirhosein Motamedi, by personally signing this document in lieu of an oath, hereby affirm that I prepared the submitted dissertation on the topic: “Advanced Retinal Optical Coherence Tomography Image Analysis in Neuroinflammatory Disorders” [“Erweiterte Bildanalyse der retinalen optischen Kohärenztomographie der Netzhaut bei neuroinflammatorischen Erkrankungen”], independently and without the support of third parties, and that I used no other sources and aids than those stated.
All parts which are based on the publications or presentations of other authors, either in letter or in spirit, are specified as such in accordance with the citing guidelines. The sections on methodology (in particular regarding practical work, laboratory regulations, statistical processing) and results (in particular regarding figures, charts and tables) are exclusively my responsibility.

My contributions to any publications to this dissertation correspond to those stated in the below joint declaration made together with the supervisor. All publications created within the scope of the dissertation comply with the guidelines of the ICMJE (International Committee of Medical Journal Editors; www.icmje.org) on authorship. In addition, I declare that I shall comply with the regulations of Charité – Universitätsmedizin Berlin on ensuring good scientific practice.

I declare that I have not yet submitted this dissertation in identical or similar form to another Faculty.

The significance of this statutory declaration and the consequences of a false statutory declaration under criminal law (Sections 156, 161 of the German Criminal Code) are known to me.”

Date Signature

Declaration of Own Contribution

Seyedamirhosein Motamedi contributed the following to the below listed publications:

Normative-Data [36]

Seyedamirhosein Motamedi, Kay Gawlik, Noah Ayadi, Hanna G. Zimmermann, Susanna Asseyer, Charlotte Bereuter, Janine Mikolajczak, Friedemann Paul, Ella-Maria Kadas, Alexander U. Brandt, **Normative Data and Minimally Detectable Change for Inner Retinal Layer Thicknesses Using a Semi-Automated OCT Image Segmentation Pipeline**, Frontiers in Neurology, 2019.

Contribution:

Seyedamirhosein Motamedi created the master table for the analysis, developed the segmentation pipeline, in particular reading, writing, and cropping of OCT images, thickness export, graphical user interface of the pipeline, and the interface connecting different parts of the pipeline, controlled OCT quality together with H.G.Z., C.B., and J.M., manually corrected layers segmentation, performed statistical analysis under supervision of A.U.B. and created tables 1, 2, and 3 based on the analysis, worked on the data interpretation together with H.G.Z., E.K., and A.U.B., created the figures, and wrote the manuscript with the help of E.K.

Foveal-Shape-Method [37]

Sunil Kumar Yadav, **Seyedamirhosein Motamedi**, Timm Oberwahrenbrock, Frederike Cosima Oertel, Konrad Polthier, Friedemann Paul, Ella Maria Kadas, Alexander U. Brandt, **CuBe: Parametric Modeling of 3D Foveal Shape Using Cubic Bézier**, Biomedical Optics Express, 2017.

Contribution:

Seyedamirhosein Motamedi contributed to the development of the foveal shape analysis method and involved in the development process from the initial idea to the publication, created the master table for the analysis, controlled the image quality of the OCT scans, and manually corrected the layers segmentation of OCT data, performed the statistical analysis and created tables 1 and 2 based on the analysis, and revised the manuscript for intellectual content.

NMOSD-Foveal-Shape [38]

Seyedamirhosein Motamedi, Frederike C. Oertel, Sunil K. Yadav, Ella M. Kadas, Margit Weise, Joachim Havla, Marius Ringelstein, Orhan Aktas, Philipp Albrecht, Klemens Ruprecht, Judith Bellmann-Strobl, Hanna G. Zimmermann, Friedemann Paul, Alexander U. Brandt, **Altered fovea in AQP4-IgG-seropositive neuromyelitis optica spectrum disorders**, Neurology-Neuroimmunology & Neuroinflammation, 2020.

Contribution:

Seyedamirhosein Motamedi created the master table for the analysis with the help of F.C.O., conducted the statistical analysis under supervision of A.U.B. and created tables 1, 2, 3, and 4 based on the analysis, contributed to the development of the foveal shape analysis method, interpreted the results together with F.C.O., J.H., H.G.Z., F.P., and A.U.B., produced the figures, and wrote the manuscript with the help of A.U.B.

Signature, date and stamp of first supervising university professor / lecturer	Signature of doctoral candidate

Copies of the Selected Publications

Motamedi, S.; Gawlik, K.; Ayadi, N.; Zimmermann, H.G.; Asseyer, S.; Bereuter, C.; Mikolajczak, J.; Paul, F.; Kadas, E.M.; Brandt, A.U. Normative Data and Minimally Detectable Change for Inner Retinal Layer Thicknesses Using a Semi-Automated OCT Image Segmentation Pipeline. Front. Neurol., 2019.
Journal Impact Factor (2019): 2.889

Yadav, S.K.; **Motamedi, S.**; Oberwahrenbrock, T.; Oertel, F.C.; Polthier, K.; Paul, F.; Kadas, E.M.; Brandt, A.U. CuBe: Parametric Modeling of 3D Foveal Shape Using Cubic Bézier. Biomed. Opt. Express, 2017.
Journal Impact Factor (2019): 3.921

Motamedi, S.; Oertel, F.C.; Yadav, S.K.; Kadas, E.M.; Weise, M.; Havla, J.; Ringelstein, M.; Aktas, O.; Albrecht, P.; Ruprecht, K.; Bellmann-Strobl, J.; Zimmermann, H.G.; Paul, F.; Brandt A.U. Altered fovea in AQP4-IgG-seropositive neuromyelitis optica spectrum disorders. Neurol Neuroimmunol Neuroinflamm, 2020.
Journal Impact Factor (2019): 7.724

Motamedi et al. Front. Neurol. 2019 (Normative-Data)

frontiers in Neurology

ORIGINAL RESEARCH
published: 25 November 2019
doi: 10.3389/fneur.2019.01117

Normative Data and Minimally Detectable Change for Inner Retinal Layer Thicknesses Using a Semi-automated OCT Image Segmentation Pipeline

Seyedamirhosein Motamedi[1], *Kay Gawlik*[1], *Noah Ayadi*[1], *Hanna G. Zimmermann*[1], *Susanna Asseyer*[1], *Charlotte Bereuter*[1], *Janine Mikolajczak*[1], *Friedemann Paul*[1,2,3], *Ella Maria Kadas*[1] *and Alexander Ulrich Brandt*[1,4]*

[1] NeuroCure Clinical Research Center, Charité-Universitätsmedizin Berlin, Corporate Member of Freie Universität Berlin, Humboldt-Universität zu Berlin, and Berlin Institute of Health, Berlin, Germany, [2] Experimental and Clinical Research Center, Max Delbrück Center for Molecular Medicine and Charité-Universitätsmedizin Berlin, Corporate Member of Freie Universität Berlin, Humboldt-Universität zu Berlin, and Berlin Institute of Health, Berlin, Germany, [3] Department of Neurology, Charité-Universitätsmedizin Berlin, Corporate Member of Freie Universität Berlin, Humboldt-Universität zu Berlin, and Berlin Institute of Health, Berlin, Germany, [4] Department of Neurology, University of California, Irvine, Irvine, CA, United States

OPEN ACCESS

Edited by:
John Jing-Wei Chen,
Mayo Clinic, United States

Reviewed by:
Jui-Kai Wang,
The University of Iowa, United States
Heather Moss,
Stanford University, United States

***Correspondence:**
Alexander Ulrich Brandt
alexander.brandt@charite.de

Specialty section:
This article was submitted to Neuro-Ophthalmology, a section of the journal Frontiers in Neurology

Received: *08 May 2019*
Accepted: *07 October 2019*
Published: *25 November 2019*

Citation:
Motamedi S, Gawlik K, Ayadi N, Zimmermann HG, Asseyer S, Bereuter C, Mikolajczak J, Paul F, Kadas EM and Brandt AU (2019) Normative Data and Minimally Detectable Change for Inner Retinal Layer Thicknesses Using a Semi-automated OCT Image Segmentation Pipeline. Front. Neurol. 10:1117. doi: 10.3389/fneur.2019.01117

Neurodegenerative and neuroinflammatory diseases regularly cause optic nerve and retinal damage. Evaluating retinal changes using optical coherence tomography (OCT) in diseases like multiple sclerosis has thus become increasingly relevant. However, intraretinal segmentation, a necessary step for interpreting retinal changes in the context of these diseases, is not standardized and often requires manual correction. Here we present a semi-automatic intraretinal layer segmentation pipeline and establish normative values for retinal layer thicknesses at the macula, including dependencies on age, sex, and refractive error. Spectral domain OCT macular 3D volume scans were obtained from healthy participants using a Heidelberg Engineering Spectralis OCT. A semi-automated segmentation tool (SAMIRIX) based on an interchangeable third-party segmentation algorithm was developed and employed for segmentation, correction, and thickness computation of intraretinal layers. Normative data is reported from a 6 mm Early Treatment Diabetic Retinopathy Study (ETDRS) circle around the fovea. An interactive toolbox for the normative database allows surveying for additional normative data. We cross-sectionally evaluated data from 218 healthy volunteers (144 females/74 males, age 36.5 ± 12.3 years, range 18–69 years). Average macular thickness (MT) was 313.70 ± 12.02 μm, macular retinal nerve fiber layer thickness (mRNFL) 39.53 ± 3.57 μm, ganglion cell and inner plexiform layer thickness (GCIPL) 70.81 ± 4.87 μm, and inner nuclear layer thickness (INL) 35.93 ± 2.34 μm. All retinal layer thicknesses decreased with age. MT and GCIPL were associated with sex, with males showing higher thicknesses. Layer thicknesses were also positively associated with each other. Repeated-measurement reliability for the manual correction of automatic intraretinal segmentation results was

excellent, with an intra-class correlation coefficient >0.99 for all layers. The SAMIRIX toolbox can simplify intraretinal segmentation in research applications, and the normative data application may serve as an expandable reference for studies, in which normative data cannot be otherwise obtained.

Keywords: optical coherence tomography (OCT), retina, normative data, inner retinal layer, segmentation, macula, healthy population, minimally detectable change

1. INTRODUCTION

Optical coherence tomography (OCT) allows non-invasive high-resolution *in vivo* imaging of the retina (1). Spectral domain OCT (SD-OCT) provides 3D volume scans of the retina, and intraretinal segmentation of macular volume scans enables quantitative OCT applications in neurodegenerative and autoimmune neuroinflammatory disorders (2, 3). The inner retinal layers, in particular, are currently of pivotal interest for several neurologic disorders. For example, the combined macular ganglion cell and inner plexiform layer (GCIPL) thickness reflects disease severity and activity in patients with multiple sclerosis (MS) (4) and is suggested for monitoring disease activity in MS (5). GCIPL might further serve to identify neurodegeneration already very early on in the disease (6), and could thus be used as a marker for assessing the individual risk of a patient at onset for an active disease course (7). GCIPL is also suggested as a sensitive marker for attack severity in acute optic neuritis (8, 9). The inner nuclear layer (INL), on the other hand, is a marker for inflammatory disease activity in MS and might be utilized to monitor treatment response (10–12). In neuromyelitis optica spectrum disorders (NMOSD), the INL might be affected as part of an autoimmune reaction against Müller cells (13), which could lead in turn to progressive GCIPL loss (14).

Intraretinal layer segmentation is a crucial step in measuring GCIPL or INL changes. In recent years, many algorithms for intraretinal layer segmentation have been developed, and are now routinely implemented in clinical OCT devices or are available as external tools for research (15). While reliability in healthy eyes is usually good (16), many scans in diseases with macroscopic retinal changes or signal quality issues caused by more difficult OCT measurement in vision-impaired individuals require quality control and manual correction (17). Proper user interfaces for manual correction of automatic segmentation results are not always available, having led to many studies with questionable OCT data based on very small regions of interest (6) or inappropriate quality control (17).

Many studies have investigated intraretinal layer thicknesses in healthy eyes to establish normative reference values, recently e.g., Invernizzi et al. (18). Clinical features like age, sex, and axial length have been reported to physiologically affect intraretinal layer thicknesses (18, 19). But normative data studies are often only applicable in a narrow context depending on the selected samples and the methodology used, and data from studies from Asia, or as a control for different diseases, are not necessarily applicable in the context of neuroinflammatory diseases in European or North American populations.

In this study we aimed (a) to establish normative values for inner intraretinal layer thicknesses in a healthy Caucasian population and age/sex distribution suitable for typical autoimmune neuroinflammatory disorders, and (b) to evaluate layer thicknesses in association with age and sex. For this task we developed an easily usable and adaptable intraretinal segmentation pipeline based on an interchangeable third-party segmentation algorithm (20) as well as a survey tool for additional normative data, which together allow data surveys also beyond the scope of this study. Both are made available as an open source application along with this publication.

2. MATERIALS AND METHODS

2.1. Study Population

We queried our institute's research database to create a normative OCT database. The database contained healthy control data from two multimodal register studies aiming to evaluate quantitative measurements of neuro-axonal damage in MS and other neuroinflammatory disorders who were recruited from July 2010 to March 2018 at the NeuroCure Clinical Research Center at the Charité-Universitätsmedizin Berlin. Each participant underwent an examination of both eyes with Spectralis SD-OCT. Retrospective inclusion criteria for the present study were participants in a healthy condition aged between 18 and 70 years, Caucasian ethnicity, and high-quality macular OCT scans (signal strength more than 15 dB). Exclusion criteria were any neurological condition, any other disorder known to affect the retina (i.e., diabetes), any eye disease affecting the retina (i.e., glaucoma), any relevant pathological finding in the neurovisual examination performed by experienced optometrists, and a refractive error above ±6 diopters. Twenty high quality macular OCT scans (signal strength more than 15 dB) of NMOSD patients all with the history of optic neuritis (ON) were randomly selected from our database to test the performance of the segmentation pipeline presented in this study.

The study was approved by the ethics committee of Charité–Universitätsmedizin Berlin and conducted according to the Declaration of Helsinki in its currently applicable version. All participants gave written informed consent.

2.2. Optical Coherence Tomography

All OCT measurements were carried out with a Spectralis SD-OCT and Heidelberg Eye Explorer (HEYEX) version 5.7.5.0 (Heidelberg Engineering, Heidelberg, Germany), by eight individual operators, with automatic real-time (ART) function for image averaging and an activated eye tracker in a dimly lit room. Macular 3D volumes were assessed by a custom scan

comprising 61 vertical B-scans (each with 768 A-Scans, with ART of 13 frames) with a scanning angle of 30 × 25° focusing on the fovea. All scans were quality controlled according to the OSCAR-IB criteria (21) and reporting adheres to APOSTEL recommendations (22). Scans not passing the quality control were excluded from analysis.

The macular scans were exported from the device and stored in HEYEX Vol file format (*.vol files), and then intraretinal segmentation was performed using the segmentation pipeline as described below. All segmentation results were quality controlled and manually corrected in case of errors by an experienced grader. In the end, the thickness data was calculated and stored in a CSV file format (.csv) for further analysis. The Early Treatment Diabetic Retinopathy Study (ETDRS) macular map, as described by the ETDRS research group (23), were used for this study. We report average macular thickness (MT), macular retinal nerve fiber layer thickness (mRNFL), combined ganglion cell and inner plexiform layer thickness (GCIPL), and inner nuclear layer thickness (INL) in the entire ETDRS macular map (the 6 mm diameter circular area around the fovea). Other layer thicknesses (e.g., outer retinal layers) and the thicknesses in different sectors of the ETDRS macular map can be studied using the provided *shiny* application and source data (**Supplementary Material**).

2.3. Intraretinal Segmentation

Intraretinal segmentation, manual correction, and thickness data export of all macular scans were done using a custom-developed intraretinal segmentation pipeline (SAMIRIX). SAMIRIX modularly includes import filters for OCT data, a third-party segmentation algorithm, a user interface for controlling and correcting segmentation results, and batch-operations for processing multiple OCT images (**Figure 1A**).

SAMIRIX was developed in MATLAB (R2017a, MathWorks, Natick, MA, USA) and the user interface OCT-Marker was written in C++11, by using Qt5, Boost, and OpenCV libraries.

2.3.1. Segmentation Algorithm

As a segmentation algorithm we used OCTLayerSegmentation (20), which has been released as a package of AURA Tools on NITRC (https://www.nitrc.org/projects/aura_tools/). We chose OCTLayerSegmentation, because it showed good performance and accuracy with an overall absolute error of 3.5 μm by combining a machine learning approach for boundary classification (random forest classification) and a robust state-of-the-art graph-cut algorithm boundary refinement (optimal graph search) in a previous study (24). OCTLayerSegmentation delineates the inner limiting membrane (ILM), external limiting membrane (ELM), Bruch membrane (BM), and the boundaries between the retinal nerve fiber layer and ganglion cell layer (RNFL-GCL), inner plexiform layer and inner nuclear layer (IPL-INL), inner nuclear layer and outer plexiform layer (INL-OPL), outer plexiform layer and outer nuclear layer (OPL-ONL), inner and outer segments (ISOS), and outer photoreceptor tips and retinal pigment epithelium (OPT-RPE) (**Figure 1B**). These

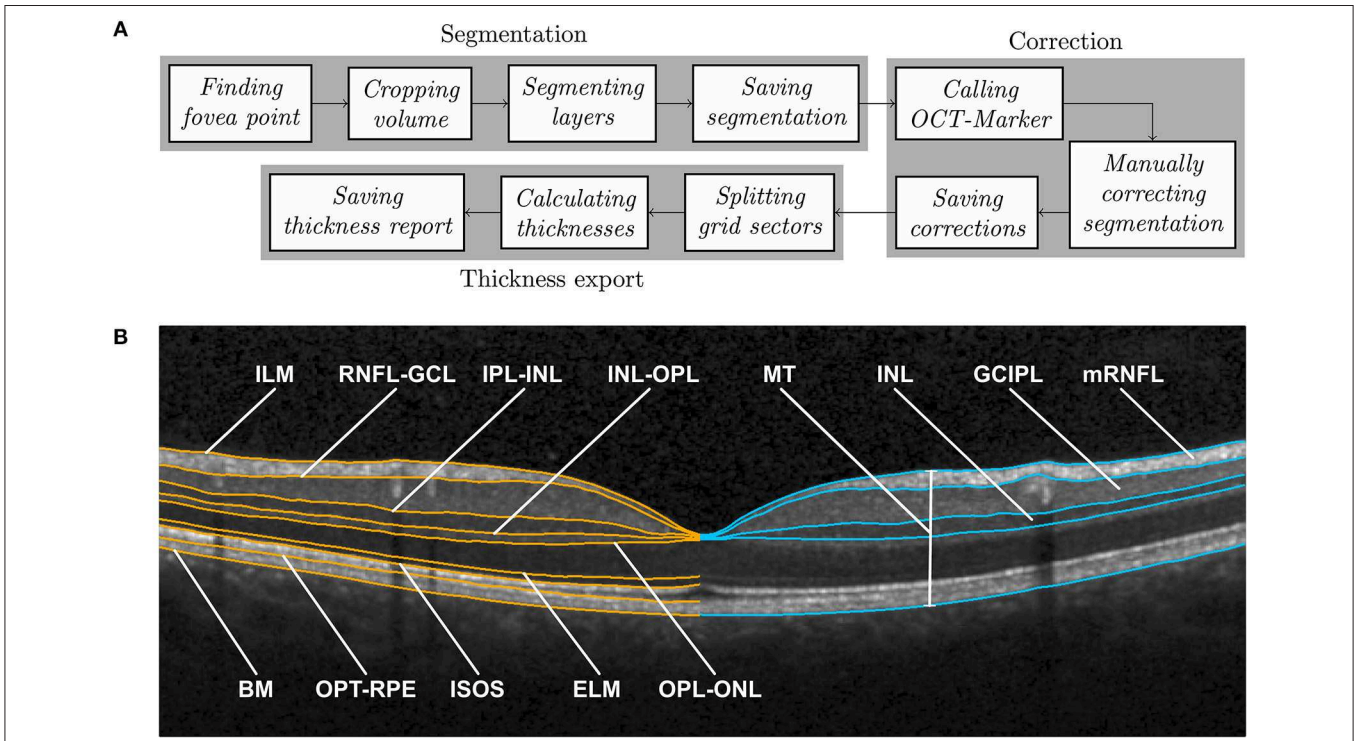

FIGURE 1 | (A) SAMIRIX pipeline, and **(B)** Boundaries delineated by layer segmentation (in orange) on the left and derived layers with manually corrected boundaries (in blue) on the right, shown on a central B-scan crossing the fovea. ILM, inner limiting membrane; RNFL, retinal nerve fiber layer; GCL, ganglion cell layer; IPL, inner plexiform layer; INL, inner nuclear layer; OPL, outer plexiform layer; ONL, outer nuclear layer; ELM, external limiting membrane; ISOS, inner and outer segments; OPT, outer photoreceptor tips; RPE, retinal pigment epithelium; BM, Bruch membrane; MT, macular thickness; mRNFL, macular retinal nerve fiber layer; GCIPL, combined ganglion cell and plexiform layer; INL, inner nuclear layer.

boundaries then serve to calculate intraretinal layer areas with nomenclature as suggested by the APOSTEL criteria (22).

For segmentation, the first step is to automatically find the central fovea point of the macular volume scan to be segmented. Based on the segmentation of the ILM and BM by the Heidelberg Engineering Eye Explorer (HEYEX) software, the height difference between the two layers is computed. In order to detect the lowest point of the foveal surface, we look at the minimum of this difference within the 1 mm circular area around the center automatically defined by HEYEX. If several minima are detected, then the median point of them is taken as the center of the foveal pit. The next step is to crop the volume to 6–6 mm square around the fovea, aligned with the main direction of the scan. This was done because many segmentation approaches work with a priori assumption regarding the expected image. The algorithm by Lang et al. used in this version of SAMIRIX works well with this volume, which was also used by the original developers of the algorithm (20). After being cropped, the volume is segmented by the integrated 3rd-party segmentation algorithm (20). The segmentation results are then read by SAMIRIX and saved alongside the volume in a single file.

2.3.2. User Interface for Manual Correction

For quality control and manual correction, we developed a graphical user interface (OCT-Marker). In the first step, the scan to be checked and corrected if necessary, is opened in OCT-Marker. A Piecewise Cubic Hermite Interpolating Polynomial (PCHIP) based correction method with defined control points is provided to the user to ease the correction process. This enables modifications on the segmentation results while going through the volume scan, B-scan by B-scan. When the correction is done, the modified segmentation is written and saved over the previous one in the data file.

2.3.3. Data Export and Batch Processing

For thickness data export, the user selects the upper and lower boundaries of the layer, and also the grid in which the thickness is going to be calculated (e.g., ETDRS 6 mm grid). Then, each volume is split into these sectors, and the average thickness of each is computed. At the end, the calculated values are written and saved in a comma separated values (csv) file.

SAMIRIX also offers the possibility of performing batch segmentation. For this purpose, the selected volumes are taken through the steps in the segmentation module, one by one. Also, in the thickness export module, the first two steps are repeated for each volume, and then the end result consists in a single thickness report saved in a single table. SAMIRIX only works with Spectralis OCT scans in HEYEX Vol file format (*.vol files). Screenshots from SAMIRIX and OCT-Marker are provided in **Supplementary Material**.

2.4. Statistical Analysis

Statistical analysis was done in R [Version 3.4.4 (25)]. Exploratory data analysis and data visualization were performed using the ggplot2 package (26). For assessment of consistency, the intra-class correlation coefficient (ICC) and 95% confidence intervals were estimated using the ICC package (27), based on the variance components from a one-way ANOVA. The coefficient of variation (CV), standard error of measurement (SEM), and minimum detectable change (MDC) for inter-rater and intra-rater consistency analysis were calculated based on the formulas described by Beckerman et al. (28). SEM and MDC, the latter sometimes also called smallest real difference (SRD), are statistical approaches to estimate the minimally needed difference between two measurements that a method is able to detect (28), and is used in this study as a measure to quantify the amount of noise. In this study, an ICC >0.9 was considered as high, between 0.8 and 0.9 as moderate, and <0.8 as insufficient, as suggested by Vaz et al. (29).

Analysis of OCT values against age, sex, and refractive error was performed by linear mixed effect models (LMM), including inter-eye within-patient correlations as a random effect [lme4 package (30), and lmerTest package (31)]. The conditional and marginal coefficients of determination were calculated with pseudo R-squared [MuMIn package (32)]. The correlation of OCT values was assessed using Pearson's product-moment correlation [stats package (25)] and regression analysis was carried out using LMM with the inclusion of inter-eye within-patient correlations as a random effect. For this study, p-values below 0.05 were considered significant.

All statistical and exploratory results of this study were established in an interactive HTML document using R Markdown (33) and Shiny (34) packages. R Markdown is a framework to run codes written in R and generates reports based on the output of the codes. By using Shiny R package, the reports can be turned into interactive web applications. The documents based on R Markdown and Shiny packages can be deployed on web servers and are therefore accessible, like web pages. A screenshot of the interactive HTML document is provided in the **Supplementary Material**.

3. RESULTS

Initially, macula scans of 438 eyes of 219 subjects were collected from our database according to the inclusion and exclusion criteria, from which the scans from 15 eyes of 14 subjects were excluded due to insufficient scan quality. Therefore, in this study, macula scans of 423 eyes of 218 subjects of Caucasian descent were included, from which 144 (66 %) subjects were females and 74 (34 %) were males. Age ranged between 18 and 69 years, with an average [±standard deviation (SD)] of 36.5 ± 12.27 years. Refractive error was available from a subset of 70 eyes (35 subjects), from which the average was -0.55 ± 1.38 SD diopter with a range between -4.75 and $+1.75$ diopter.

Table 1 provides descriptive statistics of average MT, mRNFL, GCIPL, and INL thicknesses, including the mean, SD, coefficient of variation, range, first percentile, fifth percentile, ninety-fifth percentile, and ninety-ninth percentile. **Figure 2** shows the distribution of the average layer thicknesses together with an overlaid curve representing normal distribution fitted to each graph.

Additionally, the normative (mean) thickness of the MT, mRNFL, GCIPL, and INL layers in the ETDRS macular map is

shown as heat maps in **Figure 3**, alongside the normative values of the average layer thicknesses of the eyes included in this study in the ETDRS macular map sectors. Descriptive statistics of the layer thicknesses in the ETDRS macular map sectors is provided in **Supplementary Material**.

To test inter-rater reliability, the automatic segmentation results of 44 eyes of 24 subjects from this study were manually corrected by two different experienced graders, who were masked. We then calculated the intra-class correlation coefficient (ICC) and minimum detectable change (MDC) for MT, mRNFL, GCIPL, and INL, which is detailed in **Table 2**.

TABLE 1 | Descriptive statistics of average thicknesses in the entire ETDRS macular map.

Average thickness (μm)	Mean ± SD	CV (%)	Min–Max	1st–99th percentile	5th–95th percentile
MT	313.70 ± 12.02	3.83	281.29–362.29	286.53–339.59	294.20–333.25
mRNFL	39.53 ± 3.57	9.03	30.22–54.38	32.41–49.18	34.35–45.68
GCIPL	70.81 ± 4.87	6.87	56.60–86.03	59.00–83.56	63.16–77.95
INL	35.93 ± 2.34	6.52	28.31–41.94	31.00–40.97	32.08–39.87

MT, macular thickness; mRNFL, macular retinal nerve fiber layer; GCIPL, combined ganglion cell and plexiform layer; INL, inner nuclear layer; CV, coefficient of variation; Min, minimum; Max, maximum.

Intra-rater reliability of the manual correction was tested by manually correcting the segmentation results of the same set of OCT scans from the previous reliability test (44 eyes of 24 subjects) twice by an experienced grader. The MDC (and ICC) was 0.24 (0.99994), 0.31 (0.99861), 0.23 (0.99947), and 0.19 micrometers (0.99890) for MT, mRNFL, GCIPL, and INL, respectively.

Regression analysis of layer thicknesses against age showed significant changes. In particular, MT showed an average decrease of 0.215 μm per year (p-value = 0.001). Likewise, GCIPL thickness decreased by on average 0.088 μm per year (p-value = 0.001). Significant changes of average thickness of mRNFL and INL by aging are also reported; **Table 3** provides detailed results.

Analysis of average layer thicknesses vs. sex revealed significant differences in MT and GCIPL between males and females. Males showed on average 4.18 μm higher MT than females (p-value = 0.015). Further, males had a 1.52 μm thicker GCIPL in comparison to females (p-value = 0.029). As reported in **Table 3**, neither mRNFL nor INL thickness showed significant sex differences.

Since GCIPL and INL are of particular interest, **Figure 4** shows the average GCIPL and INL thicknesses against age. The INL thickness was also plotted against the GCIPL thickness in **Figure 4**. The correlation coefficient between the INL and GCIPL thicknesses was 0.579 (p-value $< 2 \times 10^{-16}$) and the slope (B) of the linear regression was 0.277 [standard error (SE) = 0.022, p-value $< 2 \times 10^{-16}$].

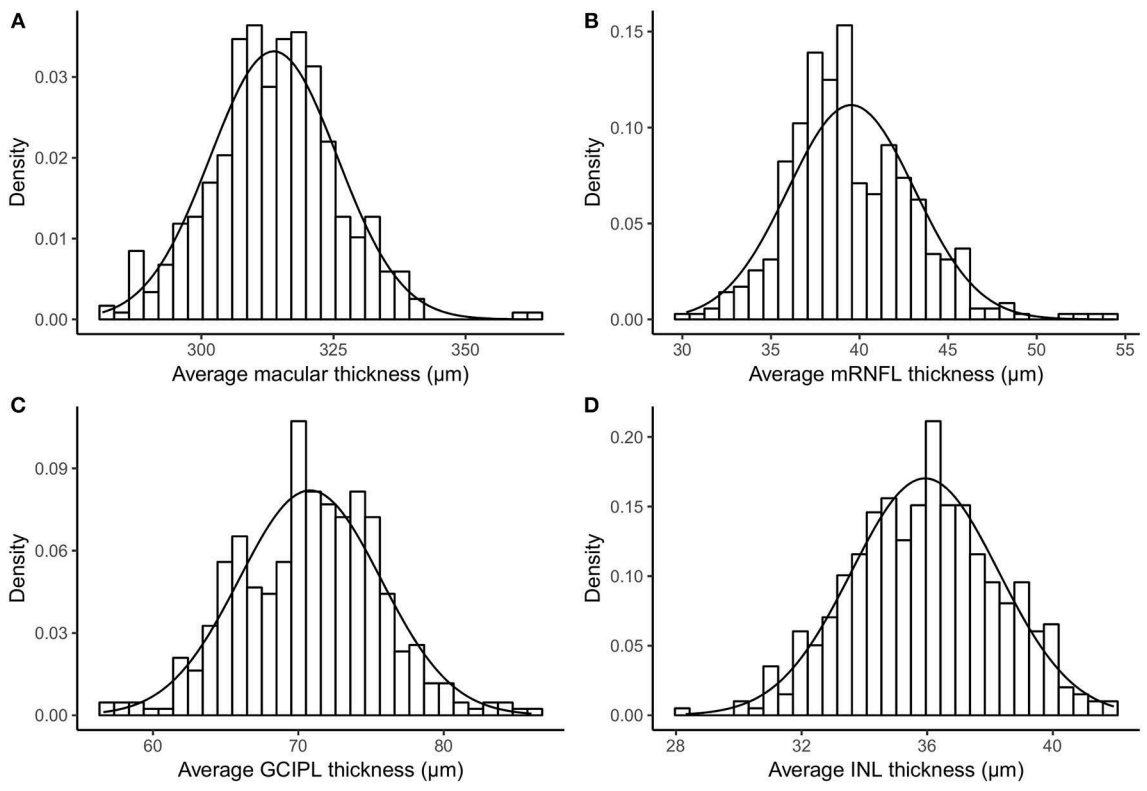

FIGURE 2 | Histogram and fitted normal distribution curve of average thickness of **(A)** macula, **(B)** mRNFL, **(C)** GCIPL, and **(D)** INL. mRNFL, macular retinal nerve fiber layer; GCIPL, combined ganglion cell and plexiform layer; INL, inner nuclear layer.

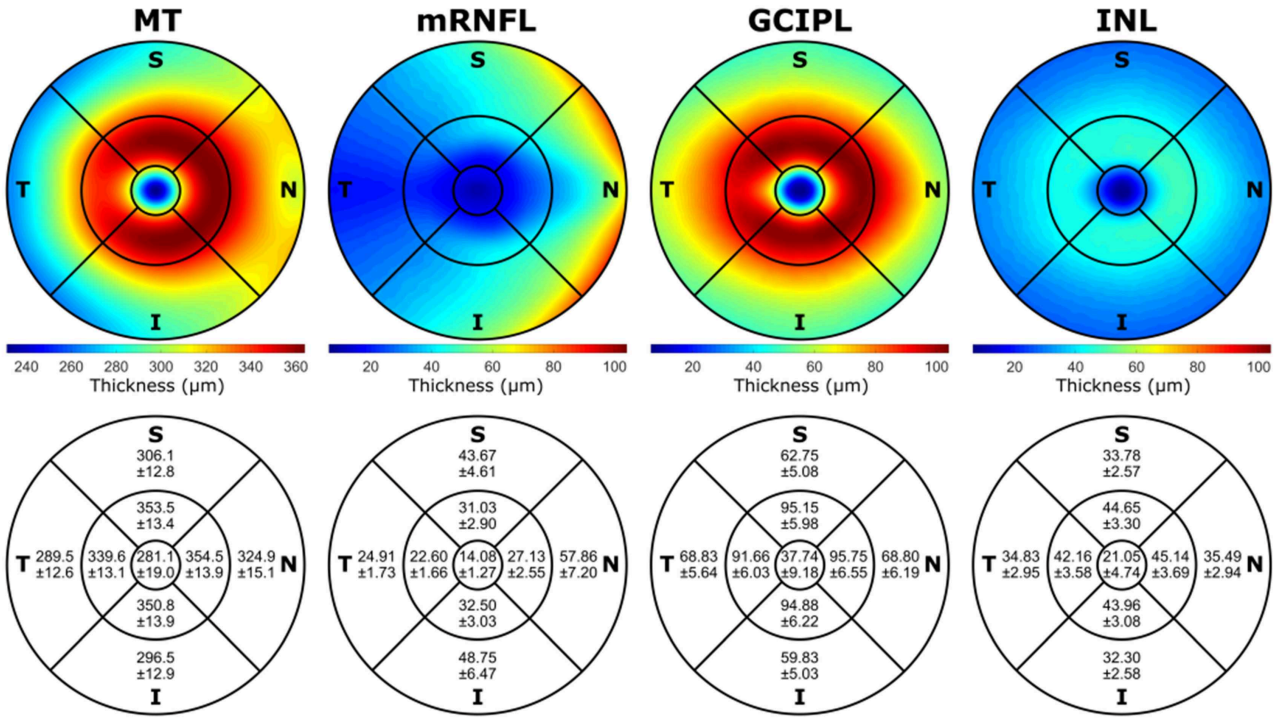

FIGURE 3 | The mean of the layer thicknesses of all the volumes included in this study in the ETDRS macular map area shown as heat maps, together with the mean and standard deviation (Mean±SD) of the average layer thicknesses in different sectors of the ETDRS macular map. The mRNFL, GCIPL, and INL heat maps have the same scale with the minimum and maximum values of all the three layers (min: 6.28 μm, max: 104.02 μm) in the interest of comparison. The left eyes were mirrored along the vertical axis, and all the images were rotated to be aligned with the fovea and center of the optic nerve head axis. All the numbers are in micrometers. MT, macular thickness; mRNFL, macular retinal nerve fiber layer; GCIPL, combined ganglion cell and plexiform layer; INL, inner nuclear layer; T, temporal; N, nasal; S, superior; I, inferior; ETDRS, Early Treatment Diabetic Retinopathy Study; Min, minimum; Max, maximum.

TABLE 2 | Inter-rater reliability measurements of segmentation corrections.

Average thickness (μm)	ICC	Upper CI	Lower CI	CV	SEM	MDC
MT	0.99984	0.99971	0.99991	0.04464	0.13728	0.38052
mRNFL	0.99350	0.98817	0.99644	0.57594	0.23771	0.65889
GCIPL	0.99794	0.99625	0.99887	0.21960	0.16519	0.45788
INL	0.99734	0.99515	0.99854	0.27271	0.10564	0.29281

MT, macular thickness; mRNFL, macular retinal nerve fiber layer; GCIPL, combined ganglion cell and plexiform layer; INL, inner nuclear layer; ICC, intra-class correlation coefficient; CI, confidence interval; CV, coefficient of variation; SEM, standard error of measurement; MDC, minimum detectable change.

To test the performance of SAMIRIX and to compare it with the performance of the HEYEX software, 20 OCT scans from NMOSD patients, all with a history of optic neuritis (ON) were segmented, and the segmentation results were manually corrected by a grader experienced in both SAMIRIX and HEYEX. The median correction time for SAMIRIX was 7:59 min (minimum: 5:07 min, maximum: 27:22 min), while the median correction time for HEYEX was 10:30 min (minimum: 8:01 min, maximum: 22:01 min). The mean absolute correction in the 6 mm ETDRS circle (the amount of correction for all the five corrected boundaries ILM, RNFL-GCL, IPL-INL, INL-OPL, and BM divided by the number of A-Scans in the 6 mm ETDRS circle) was also calculated. For the mean absolute correction in SAMIRIX, the median was 0.16 μm (minimum: 0 μm, maximum: 22.45 μm), and in HEYEX, the median was 0.79 μm (minimum: 0.06 μm, maximum: 2.02 μm).

4. DISCUSSION

In this study we present normative data for inner intraretinal layer thicknesses of a large cohort of 218 healthy subjects (423 eyes) of Caucasian ethnicity aged between 18 and 69 years, using Spectralis SD-OCT 3D macular scans.

In our study the average thickness of all investigated layers was associated with age, which is consistent with other studies (35–40). Recently, Invernizzi et al. (18) investigated the association of different intraretinal layer thicknesses in the outer and middle rings and the center of the ETDRS thickness map, with age, and showed no significant association in any regions except the center of macular thickness, which is consistent with some other studies (41, 42). von Hanno et al. (43) suggested a positive association between macular thickness and age up to around 60 years and a negative association afterwards, by studying retinal OCTs of 4,508 eyes. Previous studies investigating retinal thicknesses in relation

TABLE 3 | Regression analysis of average thicknesses against age, sex, and refractive error.

Average thickness (μm)	Against	Mean (SD)	B	SE	*P*	$R^2_{Marg.}$	$R^2_{Cond.}$
MT	Age (years)		−0.2148	0.0648	**0.0010**	0.0478	0.9679
	Sex: F vs. M	312.32 (12.11) 316.38 (11.41)	4.1771	1.6941	**0.0145**	0.0268	0.9679
	RE (diopter)		−0.3926	0.7013	0.5777	0.0030	0.9644
mRNFL	Age (years)		−0.0523	0.0192	**0.0072**	0.0312	0.8821
	Sex: F vs. M	39.46 (3.69) 39.67 (3.33)	0.3152	0.5056	0.5337	0.0017	0.8820
	RE (diopter)		−0.6067	0.2936	**0.0430**	0.0729	0.8753
GCIPL	Age (years)		−0.0874	0.0263	**0.0010**	0.0480	0.9652
	Sex: F vs. M	70.28 (4.98) 71.82 (4.48)	1.5150	0.6896	**0.0291**	0.0214	0.9652
	RE (diopter)		0.0049	0.2950	0.9869	0	0.9730
INL	Age (years)		−0.0453	0.0125	**0.0004**	0.0558	0.9331
	Sex: F vs. M	35.82 (2.40) 36.15 (2.22)	0.3526	0.3312	0.2883	0.0050	0.9331
	RE (diopter)		0.2394	0.1783	0.1841	0.0209	0.9512

MT, macular thickness; mRNFL, macular retinal nerve fiber layer; GCIPL, combined ganglion cell and plexiform layer; INL, inner nuclear layer; F, female; M, male; vs., versus; RE, refractive error; SD, standard deviation; B, slope; SE, standard error of B; P, p-*value;* $R^2_{Marg.}$*, Marginal R-squared;* $R^2_{Cond.}$*, Conditional R-Squared. Significant p-values marked in bold.*

to sex in a healthy population showed that women had thinner retinal thickness measures than men (36, 40, 41, 43, 44). Our results are in accordance with this for MT and GCIPL, but not for mRNFL and INL, which were both not sex-dependent in our cohort. The analysis using OCT data from the UK Biobank study (67,321 adults) from (45) reported associations among older age, ethnicity, BMI, smoking, and macular thickness.

Inter-rater reliability of manually corrected segmentation results was excellent with ICC values above 0.99 for all layers. MDC, from the inter-rater reliability test, was 0.46 μm for GCIPL, which is higher than the projected annual loss in healthy subjects in this study (0.09 μm per year) and similar to the average annual GCIPL loss reported in patients with MS (−1.1 μm over 2 years) (46). This means that current intraretinal segmentation is not able to reliably detect annual GCIPL loss in an individual MS patient, and further technological improvements in acquisition and image analysis are required to allow this, e.g., for clinical monitoring applications. Intraretinal segmentation of the GCIPL is, however, suited to track optic neuritis associated damage, which is often magnitudes higher than the observed MDC in this study (8, 9). For INL, the inter-rater MDC in our study was 0.29 μm, which is similar to group-wise changes reported with disease activity related effects in the range of 0.35 to 0.71 μm (12). Again, this suggests that current OCT intraretinal segmentation is not able to reliably detect meaningful INL change for this application. A previous multicenter study using the device's own semi-automatic segmentation approach with manual correction produced even higher MDC (17). While previous studies, and our current study only investigated segmentation-based reliability on a single scan, the additional acquisition noise from two different scans is likely to result in even higher MDC in a real world scenario of follow-up measurements. The reported MDC is below the resolution of the used SD-OCT technology, which suggests that imaging rather than segmentation is the limiting issue in detecting change.

To further support the opposing roles of GCIPL and INL measurements in neuroinflammatory disorders, we investigated their association in healthy controls. Both showed a moderate to strong correlation in our study, indicating that retinal thickness is reflected similarly throughout layers in an individual person. This relationship might be of relevance when interpreting GCIPL and INL in neuroinflammatory diseases, where GCIPL and INL are supposed to change in opposite directions, with GCIPL thickness reduction due to neurodegeneration (4) and INL thickening due to inflammation (12) or in response to ganglion cell loss (10).

The presented semi-automatic OCT image segmentation pipeline, SAMIRIX, provides an accessible and flexible toolbox, which can handle the entire process needed to analyze intraretinal layer thicknesses on raw SD-OCT images. SAMIRIX is not introducing a new segmentation approach, but rather implements an existing algorithm, and extends it with processing pipelines and comfortable manual correction tools. For research use, SAMIRIX was faster compared to HEYEX, and the initial segmentation more accurate. In a few cases with severely affected eyes, initial automatic segmentation produced large errors. These cases then needed more processing time than with HEYEX, suggesting a potential in improving the initial segmentation approach. Importantly, SAMIRIX offers a transparent open-source segmentation pipeline. Of note, while we compared SAMIRIX to HEYEX, there are other commercial and academic intraretinal segmentation tools available, e.g., Orion (by Voxeleron LLC, https://www.voxeleron.com/orion/) and Iowa Reference Algorithms (by Iowa Institute for Biomedical Imaging, https://www.iibi.uiowa.edu/oct-reference).

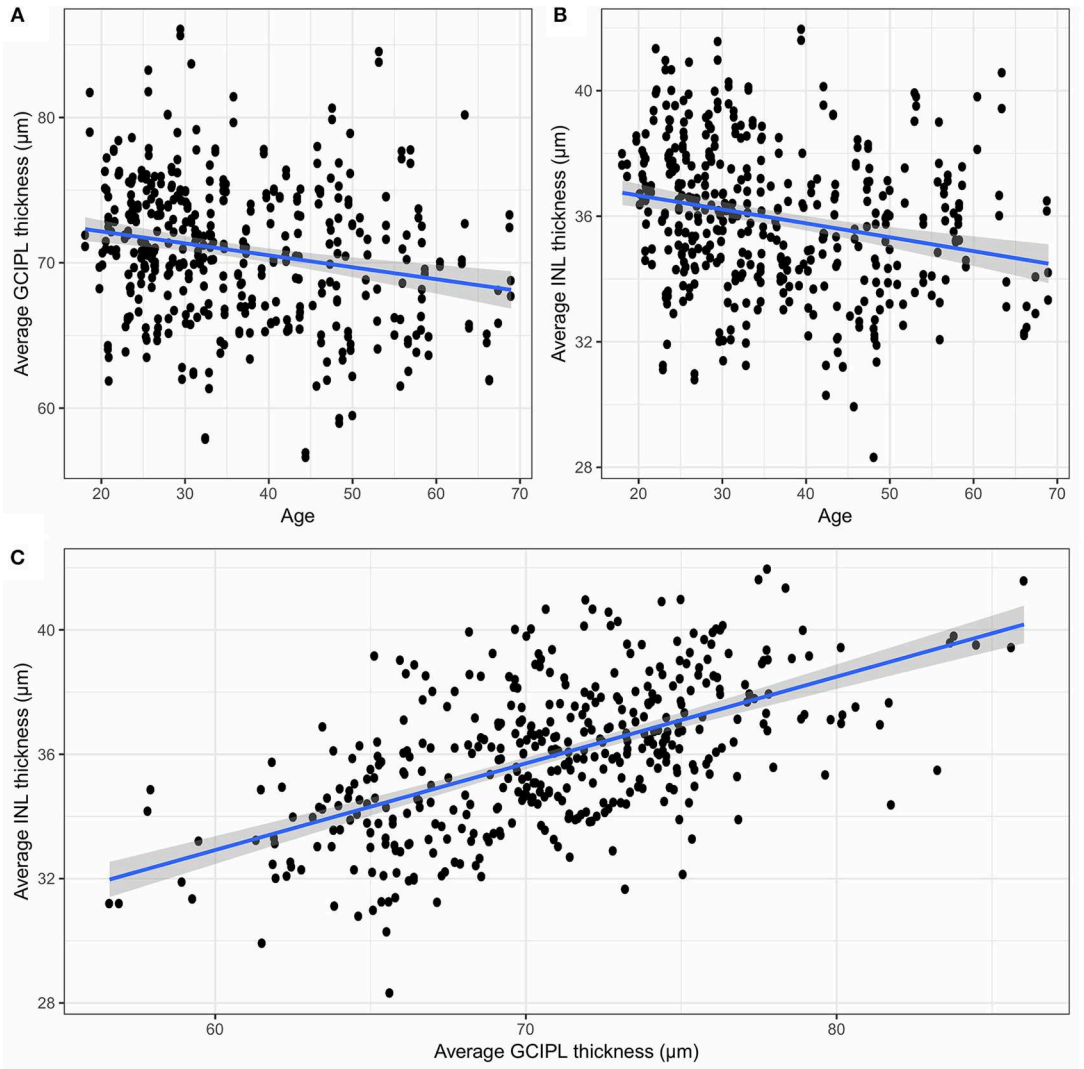

FIGURE 4 | (A) The average GCIPL thickness against age, **(B)** the average INL thickness against age, and **(C)** the average INL thickness against the average GCIPL thickness. GCIPL, combined ganglion cell and plexiform layer; INL, inner nuclear layer.

4.1. Strengths and Limitations

A general problem with reporting normative data is not only different optical properties and acquisition strategies of different devices, but also different regions of interest, which are then summarized in the respective thickness or volume measurements (47). While we report 6 mm ETDRS ring thicknesses in micrometers in this study, other regions of interest can be surveyed using the accompanying *shiny* web application. Other strengths of this study are its sample size and the similar age and sex distribution in comparison to typical cohorts of autoimmune neuroinflammatory diseases. A limitation of this study is the cross-sectional design, which impairs inferences about temporal development. The most important limitation is that we included OCT scans from only one device and one scan protocol, which limits generalizability of normative data (47). Particular caution should be taken when interpreting data acquired with various instruments, since comparative studies revealed that measurements are not directly comparable between different OCT devices (48, 49) and results can even be influenced by simple software upgrades (50). Currently, SAMIRIX is only able to work with the HEYEX Vol file format (*.vol files), which is only available through specific collaborative arrangements with Heidelberg Engineering, which is a clear limitation.

Because this study was done on a Caucasian population, readers should keep in mind that our results are not necessarily applicable to other ethnicities. Grover et al. (42) found Black subjects to have a thinner retinal thickness compared to Caucasian subjects, while Tariq et al. (51) showed that average inner macula was significantly thicker in Caucasian than East Asian and South Asian children, with South Asian children having the thinnest values. These findings were also confirmed by Girkin et al. (35), which reported that Hispanic and Indian

participants showed higher thickness compared to Europeans and Africans.

DATA AVAILABILITY STATEMENT

All analyses of this study are combined in a single R markdown code embedding R shiny interactive applications, which is provided alongside the raw data as **Supplementary Material** as well as in a public repository, in https://github.com/neurodial/am-HC-project-analysis-public.git. A copy of the source code of SAMIRIX which was used in this study and described in this paper is also provided as **Supplementary Material**. An up-to-date version of SAMIRIX can be found in a public repository with the address of https://github.com/neurodial/am_SAMIRIX.git. Additionally, the markdown HTML document was deployed to a server and is ready-to-use, available under http://shiny-apps.neurodial.de/shiny/am-HC-project-analysis-public/HC_traditional_params_markdown.Rmd with the username of "guest_user" and the password of "NeuroDiaL."

ETHICS STATEMENT

The study was approved by the ethics committee of Charité–Universitätsmedizin Berlin and conducted according to the Declaration of Helsinki in its currently applicable version. All participants gave written informed consent.

AUTHOR CONTRIBUTIONS

SM collected the data, developed SAMIRIX, manually corrected layers segmentation, performed statistical analysis, contributed to data interpretation, and wrote the manuscript. KG developed the OCT-Marker. NA contributed to the data collection and manual correction of layer segmentation. HZ contributed to the data collection, visual examinations, and data interpretation. SA contributed to the data collection and participant recruitment. CB contributed to the data collection and visual examinations. JM contributed to the data collection and visual examinations. FP contributed to the study management. EK contributed to the data interpretation and wrote the manuscript. AB planned and coordinated the study, contributed to statistical analysis and data interpretation, and reviewed the manuscript. All authors approved the final draft of the manuscript submitted for review and publication.

FUNDING

This work was supported by the Einstein Foundation Berlin (Einstein Junior Scholarship) to SM, the German Federal Ministry of Economic Affairs and Energy (BMWI EXIST 03EFEBE079) to AB, and EK, German Research Foundation (DFG Exc. 257) to FP and AB; and German Federal Ministry of Education and Research (BMBF Neu^2 ADVISIMS) to FP and AB.

ACKNOWLEDGMENTS

We thank Robyn Cunningham for her excellent technical assistance.

SUPPLEMENTARY MATERIAL

The Supplementary Material for this article can be found online at: https://www.frontiersin.org/articles/10.3389/fneur.2019.01117/full#supplementary-material

REFERENCES

1. Huang D, Swanson EA, Lin CP, Schuman JS, Stinson WG, Chang W, et al. Optical coherence tomography. *Science* (1991) 254:1178–81.
2. Oertel FC, Zimmermann H, Paul F, Brandt AU. Optical coherence tomography in neuromyelitis optica spectrum disorders: potential advantages for individualized monitoring of progression and therapy. *EPMA J.* (2017) 9:21–33. doi: 10.1007/s13167-017-0123-5
3. Oertel FC, Zimmermann HG, Brandt AU, Paul F. Novel uses of retinal imaging with optical coherence tomography in multiple sclerosis. *Expert Rev Neurother.* (2019) 19:31–43.doi: 10.1080/14737175.2019.1559051
4. Petzold A, Balcer LJ, Calabresi PA, Costello F, Frohman TC, Frohman EM, et al. Retinal layer segmentation in multiple sclerosis: a systematic review and meta-analysis. *Lancet Neurol.* (2017) 16:797–812. doi: 10.1016/S1474-4422(17)30278-8
5. Brandt AU, Martinez-Lapiscina EH, Nolan R, Saidha S. Monitoring the course of MS with optical coherence tomography. *Curr Treat Options Neurol.* (2017) 19:15.doi: 10.1007/s11940-017-0452-7
6. Oberwahrenbrock T, Ringelstein M, Jentschke S, Deuschle K, Klumbies K, Bellmann-Strobl J, et al. Retinal ganglion cell and inner plexiform layer thinning in clinically isolated syndrome. *Mult Scler J.* (2013) 19:1887–95. doi: 10.1177/1352458513489757
7. Zimmermann HG, Knier B, Oberwahrenbrock T, Behrens J, Pfuhl C, Aly L, et al. Association of retinal ganglion cell layer thickness with future disease activity in patients with clinically isolated syndrome. *JAMA Neurol.* (2018) 75:1071–9. doi: 10.1001/jamaneurol.2018.1011
8. Brandt AU, Specovius S, Oberwahrenbrock T, Zimmermann HG, Paul F, Costello F. Frequent retinal ganglion cell damage after acute optic neuritis. *Mult Scler Relat Disord.* (2018) 22:141–7. doi: 10.1016/j.msard.2018.04.006
9. Soelberg K, Specovius S, Zimmermann HG, Grauslund J, Mehlsen JJ, Olesen C, et al. Optical coherence tomography in acute optic neuritis: a population-based study. *Acta Neurol Scand.* (2018) 138:566–73. doi: 10.1111/ane.13004
10. Brandt AU, Oberwahrenbrock T, Kadas EM, Lagreze WA, Paul F. Dynamic formation of macular microcysts independent of vitreous traction changes. *Neurology.* (2014) 83:73–7. doi: 10.1212/wnl.0000000000000545
11. Kaufhold F, Zimmermann H, Schneider E, Ruprecht K, Paul F, Oberwahrenbrock T, et al. Optic neuritis is associated with inner nuclear layer thickening and microcystic macular edema independently of multiple sclerosis. *PLoS ONE.* (2013) 8:e71145. doi: 10.1371/journal.pone.0071145
12. Knier B, Schmidt P, Aly L, Buck D, Berthele A, Mühlau M, et al. Retinal inner nuclear layer volume reflects response to immunotherapy in multiple sclerosis. *Brain.* (2016) 139:2855–63. doi: 10.1093/brain/aww219
13. Oertel FC, Kuchling J, Zimmermann H, Chien C, Schmidt F, Knier B, et al. Microstructural visual system changes in AQP4-antibody–seropositive NMOSD. *Neurol Neuroimmunol Neuroinflamm.* (2017) 4:e334. doi: 10.1212/NXI.0000000000000334
14. Oertel FC, Havla J, Roca-Fernández A, Lizak N, Zimmermann H, Motamedi S, et al. Retinal ganglion cell loss in neuromyelitis optica: a longitudinal study. *J Neurol Neurosurg Psychiatry.* (2018) 89:1259–65. doi: 10.1136/jnnp-2018-318382
15. Tian J, Varga B, Tatrai E, Fanni P, Somfai GM, Smiddy WE, et al. Performance evaluation of automated segmentation software on optical coherence tomography volume data. *J Biophoton.* (2016) 9:478–89. doi: 10.1002/jbio.201500239

16. Ctori I, Huntjens B. Repeatability of foveal measurements using spectralis optical coherence tomography segmentation software. *PLoS ONE.* (2015) 10:e0129005. doi: 10.1371/journal.pone.0129005
17. Oberwahrenbrock T, Traber GL, Lukas S, Gabilondo I, Nolan R, Songster C, et al. Multicenter reliability of semiautomatic retinal layer segmentation using OCT. *Neurol Neuroimmunol Neuroinflamm.* (2018) 5:e449. doi: 10.1212/NXI.0000000000000449
18. Invernizzi A, Pellegrini M, Acquistapace A, Benatti E, Erba S, Cozzi M, et al. Normative data for retinal-layer thickness maps generated by spectral-domain OCT in a white population. *Ophthalmol Retina.* (2018) 2:808–15.e1. doi: 10.1016/j.oret.2017.12.012
19. Ooto S, Hangai M, Tomidokoro A, Saito H, Araie M, Otani T, et al. Effects of age, sex, and axial length on the three-dimensional profile of normal macular layer structures. *Investig Opthalmol Vis Sci.* (2011) 52:8769. doi: 10.1167/iovs.11-8388
20. Lang A, Carass A, Hauser M, Sotirchos ES, Calabresi PA, Ying HS, et al. Retinal layer segmentation of macular OCT images using boundary classification. *Biomed Opt Express.* (2013) 4:1133–52. doi: 10.1364/BOE.4.001133
21. Tewarie P, Balk L, Costello F, Green A, Martin R, Schippling S, et al. The OSCAR-IB consensus criteria for retinal OCT quality assessment. *PLoS ONE.* (2012) 7:e34823. doi: 10.1371/journal.pone.0034823
22. Cruz-Herranz A, Balk LJ, Oberwahrenbrock T, Saidha S, Martinez-Lapiscina EH, Lagreze WA, et al. The APOSTEL recommendations for reporting quantitative optical coherence tomography studies. *Neurology.* (2016) 86:2303–9. doi: 10.1212/WNL.0000000000002774
23. ETDRS Research Group. Grading diabetic retinopathy from stereoscopic color fundus photographs–an extension of the modified Airlie House classification. ETDRS report number 10. Early Treatment Diabetic Retinopathy Study Research Group. *Ophthalmology.* (1991) 98:786–806.
24. Oberwahrenbrock T, Jost R, Zimmermann H, Beckers I, Paul F, Brandt AU. Signal quality dependency of intra-retinal segmentation algorithms. In: *ECTRIMS Online Library* (2016). p. 146399. Available online at: https://onlinelibrary.ectrims-congress.eu/ectrims/2016/32nd/146399/timm.oberwahrenbrock.signal.quality.dependency.of.intra-retinal.segmentation.html
25. R Core Team. *R: A Language and Environment for Statistical Computing*. Vienna: R Core Team (2018). Available online at: https://www.R-project.org/
26. Wickham H. *ggplot2: Elegant Graphics for Data Analysis*. New York, NY: Springer-Verlag (2009). Available online at: http://ggplot2.org
27. Wolak ME, Fairbairn DJ, Paulsen YR. Guidelines for estimating repeatability. *Methods Ecol Evol.* (2012) 3:129–37. doi: 10.1111/j.2041-210X.2011.00125.x
28. Beckerman H, Roebroeck ME, Lankhorst GJ, Becher JG, Bezemer PD, Verbeek AL. Smallest real difference, a link between reproducibility and responsiveness. *Qual Life Res.* (2001) 10:571–8. doi: 10.1023/a:1013138911638
29. Vaz S, Falkmer T, Passmore AE, Parsons R, Andreou P. The case for using the repeatability coefficient when calculating test–retest reliability. *PLoS ONE.* (2013) 8:e73990. doi: 10.1371/journal.pone.0073990
30. Bates D, Mächler M, Bolker B, Walker S. Fitting linear mixed-effects models using lme4. *J Stat Softw.* (2015) 67:1–48. doi: 10.18637/jss.v067.i01
31. Kuznetsova A, Brockhoff PB, Christensen RHB. lmerTest package: tests in linear mixed effects models. *J Stat Softw.* (2017) 82:1–26. doi: 10.18637/jss.v082.i13
32. Barton K. *MuMIn: Multi-Model Inference* (2018). R package version 1.40.4. Available online at: https://CRAN.R-project.org/package=MuMIn
33. Allaire J, Horner J, Marti V, Porte N. *Markdown: 'Markdown' Rendering for R; 2017*. R package version 0.8. Available online at: https://CRAN.R-project.org/package=markdown
34. Chang W, Cheng J, Allaire J, Xie Y, McPherson J. *Shiny: Web Application Framework for R* (2017). R package version 1.0.5. Available online at: https://CRAN.R-project.org/package=shiny
35. Girkin CA, McGwin G, Sinai MJ, Sekhar GC, Fingeret M, Wollstein G, et al. Variation in optic nerve and macular structure with age and race with spectral-domain optical coherence tomography. *Ophthalmology.* (2011) 118:2403–8. doi: 10.1016/j.ophtha.2011.06.013
36. Gupta P, Sidhartha E, Tham YC, Chua DKP, Liao J, Cheng CY, et al. Determinants of macular thickness using spectral domain optical coherence tomography in healthy eyes: the Singapore Chinese eye study. *Investig Opthalmol Vis Sci.* (2013) 54:7968. doi: 10.1167/iovs.13-12436
37. Mitkova-Hristova VT, Konareva-Kostyaneva MI. Macular thickness measurements in healthy eyes using spectral optical coherence tomography. *Folia Med.* (2011) 53:28–33. doi: 10.2478/v10153-011-0064-z
38. Myers CE, Klein BEK, Meuer SM, Swift MK, Chandler CS, Huang Y, et al. Retinal thickness measured by spectral-domain optical coherence tomography in eyes without retinal abnormalities: the Beaver dam eye study. *Am J Ophthalmol.* (2015) 159:445–56.e1. doi: 10.1016/j.ajo.2014.11.025
39. Nieves-Moreno M, de-la Casa JMM, Morales-Fernández L, Sánchez-Jean R, Sáenz-Francés F, García-Feijoó J. Impacts of age and sex on retinal layer thicknesses measured by spectral domain optical coherence tomography with spectralis. *PLoS ONE.* (2018) 13:e0194169. doi: 10.1371/journal.pone.0194169
40. Song WK, Lee SC, Lee ES, Kim CY, Kim SS. Macular thickness variations with sex, age, and axial length in healthy subjects: a spectral domain–optical coherence tomography study. *Investig Opthalmol Vis Sci.* (2010) 51:3913. doi: 10.1167/iovs.09-4189
41. Adhi M, Aziz S, Muhammad K, Adhi MI. Macular thickness by age and gender in healthy eyes using spectral domain optical coherence tomography. *PLoS ONE.* (2012) 7:e37638. doi: 10.1371/journal.pone.0037638
42. Grover S, Murthy RK, Brar VS, Chalam KV. Normative data for macular thickness by high-definition spectral-domain optical coherence tomography (spectralis). *Am J Ophthalmol.* (2009) 148:266–71. doi: 10.1016/j.ajo.2009.03.006
43. von Hanno T, Lade AC, Mathiesen EB, Peto T, Njølstad I, Bertelsen G. Macular thickness in healthy eyes of adults (N = 4508) and relation to sex, age and refraction: the Tromsø Eye Study (2007–2008). *Acta Ophthalmol.* (2016) 95:262–9. doi: 10.1111/aos.13337
44. Duan XR, Liang YB, Friedman DS, Sun LP, Wong TY, Tao QS, et al. Normal macular thickness measurements using optical coherence tomography in healthy eyes of adult Chinese persons: the Handan eye study. *Ophthalmology.* (2010) 117:1585–94. doi: 10.1016/j.ophtha.2009.12.036
45. Patel PJ, Foster PJ, Grossi CM, Keane PA, Ko F, Lotery A, et al. Spectral-domain optical coherence tomography imaging in 67,321 adults. *Ophthalmology.* (2016) 123:829–40. doi: 10.1016/j.ophtha.2015.11.009
46. Balk LJ, Cruz-Herranz A, Albrecht P, Arnow S, Gelfand JM, Tewarie P, et al. Timing of retinal neuronal and axonal loss in MS: a longitudinal OCT study. *J Neurol.* (2016) 263:1323–31.doi: 10.1007/s00415-016-8127-y
47. Oberwahrenbrock T, Weinhold M, Mikolajczak J, Zimmermann H, Paul F, Beckers I, et al. Reliability of intra-retinal layer thickness estimates. *PLoS ONE.* (2015) 10:e0137316. doi: 10.1371/journal.pone.0137316
48. Pierro L, Giatsidis SM, Mantovani E, Gagliardi M. Macular thickness interoperator and intraoperator reproducibility in healthy eyes using 7 optical coherence tomography instruments. *Am J Ophthalmol.* (2010) 150:199–204.e1. doi: 10.1016/j.ajo.2010.03.015
49. Seigo MA, Sotirchos ES, Newsome S, Babiarz A, Eckstein C, Ford E, et al. *In vivo* assessment of retinal neuronal layers in multiple sclerosis with manual and automated optical coherence tomography segmentation techniques. *J Neurol.* (2012) 259:2119–30. doi: 10.1007/s00415-012-6466-x
50. Coric D, Petzold A, Uitdehaag BMJ, Balk LJ. Software updates of OCT segmentation algorithms influence longitudinal assessment of retinal atrophy. *J Neurol Sci.* (2018) 387:16–20. doi: 10.1016/j.jns.2018.01.020
51. Tariq YM, Li H, Burlutsky G, Mitchell P. Ethnic differences in macular thickness. *Clin Exp Ophthalmol.* (2011) 39:893–8. doi: 10.1111/j.1442-9071.2011.02593.x

Conflict of Interest: EK, FP, and AB are co-founders and hold shares in technology start-up Nocturne GmbH, which has commercial interest in OCT applications in neurology. EK is now an employee of Nocturne.

The remaining authors declare that the research was conducted in the absence of any commercial or financial relationships that could be construed as a potential conflict of interest.

Copyright © 2019 Motamedi, Gawlik, Ayadi, Zimmermann, Asseyer, Bereuter, Mikolajczak, Paul, Kadas and Brandt. This is an open-access article distributed under the terms of the Creative Commons Attribution License (CC BY). The use, distribution or reproduction in other forums is permitted, provided the original author(s) and the copyright owner(s) are credited and that the original publication in this journal is cited, in accordance with accepted academic practice. No use, distribution or reproduction is permitted which does not comply with these terms.

Yadav et al. Biomed. Opt. Express 2017 (Foveal-Shape-Method)

The publication

Sunil Kumar Yadav, **Seyedamirhosein Motamedi**, Timm Oberwahrenbrock, Frederike Cosima Oertel, Konrad Polthier, Friedemann Paul, Ella Maria Kadas, Alexander U. Brandt, **CuBe: Parametric Modeling of 3D Foveal Shape Using Cubic Bézier**, Biomedical Optics Express, 2017,

is available under:

https://dx.doi.org/10.1364%2FBOE.8.004181

Motamedi et al. N2 2020 (NMOSD-Foveal-Shape)

ARTICLE OPEN ACCESS

Altered fovea in AQP4-IgG–seropositive neuromyelitis optica spectrum disorders

Seyedamirhosein Motamedi, MSc, Frederike C. Oertel, MD, Sunil K. Yadav, PhD, Ella M. Kadas, PhD, Margit Weise, MSc, Joachim Havla, MD, Marius Ringelstein, MD, Orhan Aktas, MD, Philipp Albrecht, MD, Klemens Ruprecht, MD, Judith Bellmann-Strobl, MD, Hanna G. Zimmermann, PhD, Friedemann Paul, MD, and Alexander U. Brandt, MD

Correspondence
Dr. Brandt
alexander.brandt@charite.de

Neurol Neuroimmunol Neuroinflamm 2020;7:e805. doi:10.1212/NXI.0000000000000805

Abstract

Objective

To investigate disease-specific foveal shape changes in patients with neuromyelitis optica spectrum disorders (NMOSDs) using foveal morphometry.

Methods

This cross-sectional study included macular spectral domain optical coherence tomography scans of 52 eyes from 28 patients with aquaporin-4 immunoglobulin G (AQP4-IgG)-seropositive NMOSD, 116 eyes from 60 patients with MS, and 123 eyes from 62 healthy controls (HCs), retrospectively, and an independent confirmatory cohort comprised 33/33 patients with NMOSD/MS. The fovea was characterized using 3D foveal morphometry. We included peripapillary retinal nerve fiber layer (pRNFL) thickness and combined macular ganglion cell and inner plexiform layer (GCIPL) volume to account for optic neuritis (ON)-related neuroaxonal damage.

Results

Group comparison showed significant differences compared with HC in the majority of foveal shape parameters in NMOSD, but not MS. Pit flat disk area, average pit flat disk diameter, inner rim volume, and major slope disk length, as selected parameters, showed differences between NMOSD and MS (p value = 0.017, 0.002, 0.005, and 0.033, respectively). This effect was independent of ON. Area under the curve was between 0.7 and 0.8 (receiver operating characteristic curve) for discriminating between NMOSD and MS. Pit flat disk area and average pit flat disk diameter changes independent of ON were confirmed in an independent cohort.

Conclusions

Foveal morphometry reveals a wider and flatter fovea in NMOSD in comparison to MS and HC. Comparison to MS and accounting for ON suggest this effect to be at least in part independent of ON. This supports a primary retinopathy in AQP4-IgG–seropositive NMOSD.

From the Experimental and Clinical Research Center (S.M., F.C.O., J.B.-S., H.G.Z., F.P., A.U.B.), Max-Delbrück Center for Molecular Medicine and Charité - Universitätsmedizin Berlin, corporate member of Freie Universität Berlin, Humboldt-Universität zu Berlin, and Berlin Institute of Health; NeuroCure Clinical Research Center (S.M., F.C.O., S.K.Y., E.M.K., J.B.-S., H.G.Z., F.P., A.U.B.), Charité – Universitätsmedizin Berlin, corporate member of Freie Universität Berlin, Humboldt-Universität zu Berlin, and Berlin Institute of Health, Germany; Division of Neuroinflammation and Glial Biology (F.C.O.), University of California, San Francisco; Nocturne GmbH (S.K.Y., E.M.K.), Berlin; Department of Neurology (M.W., M.R., O.A., P.A.), Medical Faculty, Heinrich Heine University, Düsseldorf; Institute of Clinical Neuroimmunology (J.H.), LMU Hospital, Ludwig-Maximilians University, Munich; Department of Neurology (M.R.), Center for Neurology and Neuropsychiatry, LVR-Klinikum Düsseldorf; Department of Neurology (K.R., F.P.), Charité - Universitätsmedizin Berlin, corporate member of Freie Universität Berlin, Humboldt-Universität zu Berlin, and Berlin Institute of Health, Germany; and Department of Neurology (A.U.B.), University of California, Irvine.

Go to Neurology.org/NN for full disclosures. Funding information is provided at the end of the article.

The Article Processing Charge was funded by the authors.

This is an open access article distributed under the terms of the Creative Commons Attribution-NonCommercial-NoDerivatives License 4.0 (CC BY-NC-ND), which permits downloading and sharing the work provided it is properly cited. The work cannot be changed in any way or used commercially without permission from the journal.

Copyright © 2020 The Author(s). Published by Wolters Kluwer Health, Inc. on behalf of the American Academy of Neurology.

Glossary

AQP4-IgG = aquaporin-4 immunoglobulin G; **ART** = automatic real time; **AUC** = area under the curve; **B** = estimate; **FT** = foveal thickness; **GCIPL** = combined macular ganglion cell and inner plexiform layer; **HC** = healthy control; **ILM** = inner limiting membrane; **INL** = inner nuclear layer; **MOG** = myelin oligodendrocyte glycoprotein; **NMOSD** = neuromyelitis optica spectrum disorder; **OCT** = optical coherence tomography; **ON** = optic neuritis; **ON−** = eyes without a history of ON; **ON+** = eyes with a history of ON; **pRNFL** = peripapillary retinal nerve fiber layer; **ROC** = receiver operating characteristic; **SE** = standard error of B.

Aquaporin-4 immunoglobulin G (AQP4-IgG)-seropositive neuromyelitis optica spectrum disorder (NMOSD) is an inflammatory astrocytopathy defined by pathogenic serum immunoglobulin G antibodies against aquaporin-4.[1–3]

Optic neuritis (ON) is a hallmark of NMOSD and leads to severe neuroaxonal damage in optic nerve and retina associated with oftentimes severe vision loss.[4–8] Retinal optical coherence tomography (OCT) can be used to measure this damage[9–12]: Peripapillary retinal nerve fiber layer (pRNFL) and combined macular ganglion cell and inner plexiform layer (GCIPL) typically become thinner, whereas inner nuclear layer (INL) becomes thicker as a result of ON.[6,13–15]

Recently, a foveal thickness (FT) reduction has been reported in eyes never experiencing an ON in patients with AQP4-IgG–seropositive NMOSD,[16,17] suggesting either subclinical optic nerve inflammation or primary retinal astrocytopathy in NMOSD.[8] This change in FT appeared to be driven by a change in foveal shape, with a normally V-shaped fovea appearing more widened and U-shaped with flattened disk in eyes of patients with AQP4-IgG–seropositive NMOSD.[17]

Because FT is a weak measure for foveal shape, we developed a 3D foveal morphometry method, which we previously described and validated in detail.[18] Here, we use this approach to investigate the foveal shape in patients with AQP4-IgG–seropositive NMOSD. We compare findings against measurements in patients with MS, which also presents with ON, and against healthy controls (HCs). Our goal was to investigate whether foveal changes are characteristic to AQP4-IgG–seropositive NMOSD and not simply caused by ON.

Methods

Study population

In this analysis, we retrospectively included data from an ongoing observational cohort study in patients with NMOSD at the NeuroCure Clinical Research Center at Charité—Universitätsmedizin Berlin, Germany, acquired from August 2013 to November 2016. Inclusion criteria were a minimum age of 18 years and fulfilling the diagnostic criteria for AQP4-IgG–seropositive NMOSD according to the 2015 International Consensus Diagnostic Criteria.[7] AQP4-IgG–seropositivity was tested using a cell-based assay (Euroimmun, Lübeck, Germany). Exclusion criteria were any other neurologic or ophthalmologic disorder (e.g., glaucoma, diabetes, and refractive error >6 diopters), which can affect the retina.[19] Eyes with an episode of ON within the last 6 months before the OCT examinations were excluded. Of 46 patients enclosed in the study, we included 28 patients with NMOSD in the analysis after applying the inclusion and exclusion criteria (table 1). We additionally included 60 patients with relapsing-remitting MS according to the 2010 revised McDonald criteria,[20] from 2 cohort studies about MS and clinically isolated syndrome and 62 HCs, both groups age and sex matched to the NMOSD cohort, in this study (table 1). Data from 17 patients with AQP4-IgG–seropositive NMOSD (61%) were already included in a previous study by Oertel et al.[17] High-contrast visual acuity was measured using Early Treatment in Diabetes Retinopathy Study charts at a 4-m distance with an Optec 6500 P system (Stereo Optical, Chicago, IL), with best correction and under photopic conditions.

A confirmatory cohort consisting of macular OCTs from 58 eyes of 33 patients with AQP4-IgG–seropositive NMOSD (eyes with a history of ON [ON+]: 27; 33 women; age: 49.2 ± 15.4 years) and 62 eyes of 33 patients with MS (ON+: 12; 32 women; age: 49.7 ± 14.7 years) from longitudinal prospective observational cohort studies at the Department of Neurology, Universitätsklinikum Düsseldorf at Heinrich Heine University, Düsseldorf, Germany, was included in this study, following the same inclusion and exclusion criteria. MS and NMOSD groups were well matched in this cohort for age ($p = 0.812$) and sex ($p = 1$), but not for the proportion of eyes with ON ($p = 0.001$). The NMOSD group is well matched to the Berlin cohort for age ($p = 0.113$), sex ($p = 0.214$), and ON+ ($p = 0.507$).

Ethics statement

The study was approved by the local ethics committee at Charité—Universitätsmedizin Berlin (EA1/131/09, EA1/163/12, and EA1/182/10). The confirmatory OCT data were collected under approval from the local ethics committee at Heinrich Heine University Düsseldorf (4389R). The study was conducted according to the Declaration of Helsinki in its currently applicable version and the applicable German and European laws. All the participants gave written informed consent.

Optical coherence tomography

All retinal OCT images (exploratory and confirmatory cohort) were taken using Spectralis spectral domain OCT devices from Heidelberg Engineering (Heidelberg, Germany), with activated eye tracker and automatic real-time (ART) averaging. The pRNFL thickness was calculated using standard ring scans around the optic nerve head (12°, single B

Table 1 Demographic description of NMOSD, MS, and HC cohorts

	NMOSD	MS	HC
No. of patients (N)	28	60	62
No. of eyes (N)	52	116	123
Sex (female) (N [%])[a]	26 (93%)	55 (92%)	56 (90%)
Age (y) (mean ± SD)[b]	43.6 ± 11.5	39.0 ± 10.9	41.7 ± 13.5
Patients with a history of ON (N [%])	16 (57%)	29 (48%)	—
Eyes with a history of ON (N [%])[c]	20 (38%)	32 (28%)	—
Number of ONs per eye (median [range])	1.5 (1–8)	1 (1–2)	—
VA for ON eyes (logMAR) (mean ± SD)[d]	0.36 ± 0.69	−0.09 ± 0.10	
EDSS score (median [range])	3 (0–6.5)	2 (0–4.5)	—
Disease duration (y) (mean ± SD)	6.8 ± 4.8	7.9 ± 8.4	—
pRNFL (μm) (mean ± SD)	81.2 ± 22.1	90.8 ± 15.3	97.6 ± 8.8
GCIPL (mm^3) (mean ± SD)	1.69 ± 0.29	1.83 ± 0.24	1.94 ± 0.14
INL (mm^3) (mean ± SD)	0.94 ± 0.09	0.96 ± 0.06	0.95 ± 0.06
FT (μm) (mean ± SD)	262.9 ± 14.9	272.1 ± 20.3	272.3 ± 23.1

Abbreviations: EDSS = Expanded Disability Status Scale; FT = foveal thickness; GCIPL = combined macular ganglion cell and inner plexiform layer volume; HC = healthy controls; INL = inner nuclear layer volume; logMAR = logarithm of the minimum angle of resolution; NMOSD = neuromyelitis optica spectrum disorders; ON = optic neuritis; pRNFL = peripapillary retinal nerve fiber layer thickness; VA = high-contrast visual acuity.
[a] Sex match: p value = 1.
[b] Age match: p value: HC vs MS = 0.382, HC vs NMOSD = 0.437, MS vs NMOSD = 0.056.
[c] ON match: p value = 0.199.
[d] VA measurements for 25 (78%) ON eyes of patients with MS and 17 (85%) ON eyes of patients with NMOSD were available.

scan with 1536 A scans, 16 ≤ ART ≤100). The volume of the GCIPL and INL was calculated in a 6-mm diameter around the fovea, and FT was measured in a 1-mm-diameter area around the fovea, based on macular volume scans (25° × 30°, 61 B scans with 768 A scans per each B scan, ART = 15). Intraretinal layer segmentation was performed and corrected if needed using Heidelberg Eye Explorer (HEYEX version 1.9.10.0) by an experienced grader. All OCT scans were quality controlled according to the OSCAR-IB criteria,[19,21] and OCT data are reported in accordance with the Advised Protocol for OCT Study Terminology and Elements (APOSTEL) recommendations.[22] Four eyes from the exploratory cohort were excluded from the study because of inadequate OCT scan quality.

Foveal morphometry

All macular volume OCTs were analyzed using a 3D foveal morphometry described previously in detail.[18] In brief, first, the 3D macular scan is flattened based on the segmentation of the Bruch membrane as the reference plane, and then the inner limiting membrane (ILM) surface is smoothed and reconstructed radially using a cubic Bezier polynomial model. Based on the reconstructed ILM surface, several parameters are defined to describe the foveal and parafoveal shape. Three surfaces are defined in this foveal shape analysis method: rim disk, which connects the points on the surface with the maximum height (rim points); slope disk, which connects the points with the maximum slopes in the parafoveal area; and pit flat disk, which characterizes the flatness of the foveal pit. Each surface is described by 4 parameters—the length in the dominant direction (major axis): major length; the length in the second dominant direction (perpendicular to the major axis): minor length; the area; and the average diameter. In addition, the distance between the fovea (the minimum point) and the center of rim disk: average pit depth; the distance between the fovea and the reference plane: central foveal thickness; the average height of the rim points: average rim height; the volume between the ILM surface and the reference plane: rim volume; the volume between the ILM surface and rim disk: pit volume; the volume between the ILM surface and the reference plane within 1-mm-diameter cylinder centered at the fovea: inner rim volume; and the average slope at the maximum slope points: average maximum pit slope are measured by this method to characterize the 3D foveal shape. Figure 1 gives an overview of the method and the defined parameters. Test-retest reliability was excellent in all foveal morphometry parameters with intraclass correlation coefficients >0.9 in all cases (table e-1, links.lww.com/NXI/A270).

Statistical analysis

Sex and ON differences between groups were tested using χ^2 tests, and age differences were tested using 2-sample Wilcoxon tests. Performance measurements were based on the area under the curve (AUC) for receiver operating

Figure 1 Three-dimensional foveal shape analysis method overview

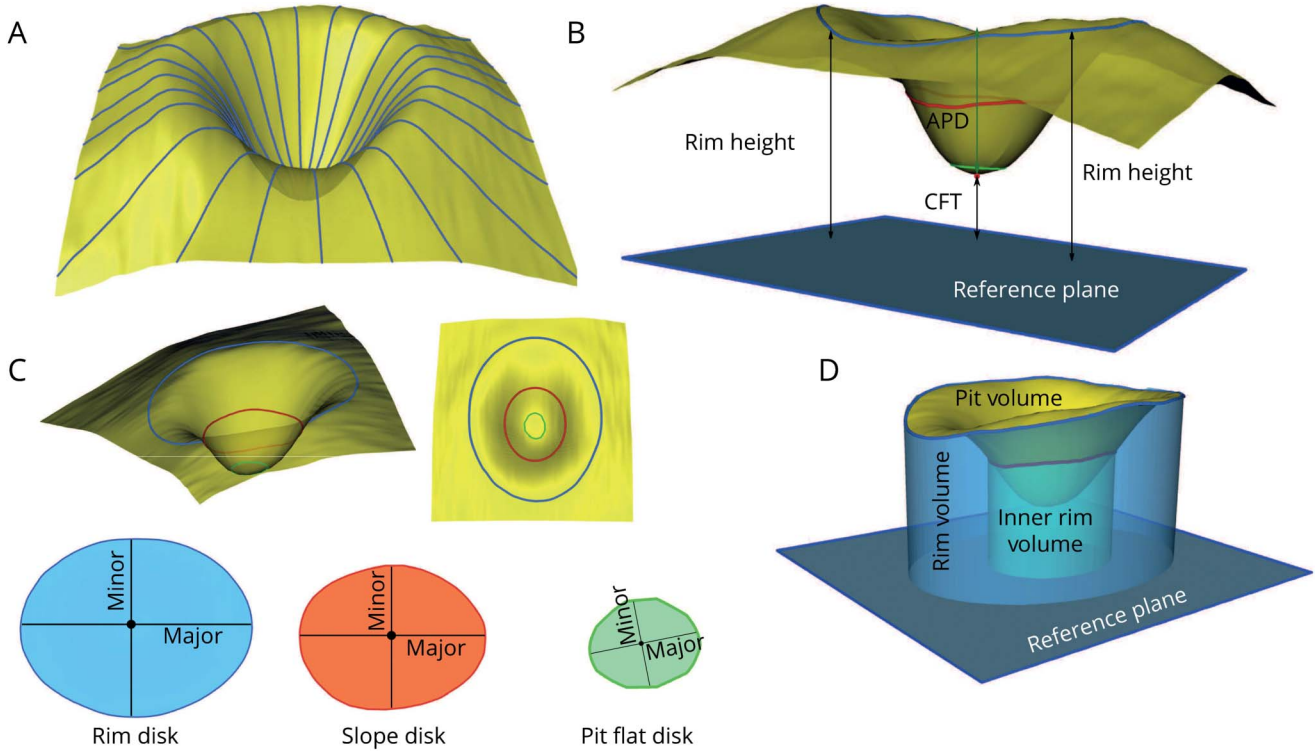

(A) ILM surface smoothing and radial reconstruction using the cubic Bezier polynomial. (B) Rim height, average pit depth, and central foveal thickness. (C) Rim disk (blue), slope disk (red), and pit flat disk (green) and major and minor axes on each surface. (D) Rim volume, pit volume, and inner rim volume. APD = average pit depth, CFT = central foveal thickness; ILM = inner limiting membrane; major = major axis; minor = minor axis.

characteristic (ROC) curves. All linear regression analyses were performed using linear mixed-effect models including intereye within-patient correlations, age, and sex as random effects. The marginal and conditional coefficients of determination of the linear models were calculated with pseudo R-squared. Stepwise logistic regression analysis for model selection was performed by the Akaike Information Criteria with both backward and forward modes of stepwise search based on generalized linear models. In this exploratory study, we corrected p values for multiple testing using the Benjamini-Hochberg procedure. In addition, the identified parameter differences were tested in a second independent cohort obtained with the same scanning protocol at a different center. One-sided p values were reported for the confirmatory cohort, not corrected for multiple testing. Sample size for the confirmatory cohort was calculated for 1-sided 2-sample t-test with 90% power and a significance level of 0.05. To adjust this estimate for eye-based statistics, we added 60% sample size to account for intereye within-patient effects and additional covariates. All statistical analysis were performed in R version 3.5.0[23] with packages stats, lme4, lmerTest, MuMIn, ROCR, ggplot2, plotROC, pwr, multcomp, and ggpubr packages. The p values less than 0.05 were considered significant.

Data availability

All data are available on reasonable request from the corresponding author.

Results

Foveal shape changes in NMOSD and MS

First, we analyzed foveal shape in patients with NMOSD and MS and compared results with measurements in HCs. Foveal shape was altered in patients with NMOSD, but only mildly affected in patients with MS, both in comparison to HCs (table 2). Foveal parameters stratified by history of ON are included in supplemental data (table e-2, links.lww.com/NXI/A271).

In contrast, both patients with MS and NMOSD showed neuroaxonal damage typically occurring after ON: pRNFL and GCIPL were lower in patients with NMOSD in comparison to HCs (pRNFL: standard error of B [SE] = −17.7 [3.0] μm, $p < 0.001$, GCIPL: B [SE] = −0.27 [0.04] mm^3, $p < 0.001$), but also in patients with MS in comparison to HCs (pRNFL: B [SE] = −7.0 (2.0) μm, $p < 0.001$, GCIPL: B [SE] = −0.12 [0.03] mm^3, $p = 0.001$).

Parameter selection

Next, we selected parameters with the highest potential to be abnormal in NMOSD: We therefore analyzed parameter performance in discriminating between eyes from patients with NMOSD and MS, regardless of ON status (table 3 and figure 2A). This was followed by a linear regression analysis against diagnosis, history of ON, and their interaction effect to derive effect sizes and group differences accounting for ON.

Table 2 Foveal shape analysis parameters results (mean ± SD) and linear regression analysis for NMOSD and MS vs HC

	HC (mean ± SD)	MS (mean ± SD)	NMOSD (mean ± SD)	HC vs NMOSD		HC vs MS	
				B (SE)	*p*	B (SE)	*p*
Average pit depth (mm)	0.117 ± 0.021	0.111 ± 0.018	0.101 ± 0.026	−0.017 (0.005)	**<0.001**	−0.006 (0.003)	0.078
Central foveal thickness (mm)	0.231 ± 0.015	0.229 ± 0.017	0.228 ± 0.017	−0.004 (0.004)	0.330	−0.002 (0.003)	0.535
Average rim height (mm)	0.348 ± 0.014	0.340 ± 0.016	0.328 ± 0.018	−0.021 (0.003)	**<0.001**	−0.009 (0.002)	**<0.001**
Average rim disk diameter (mm)	2.184 ± 0.115	2.152 ± 0.110	2.132 ± 0.130	−0.056 (0.027)	**0.037**	−0.034 (0.020)	0.082
Rim disk area (mm^2)	3.717 ± 0.387	3.606 ± 0.371	3.545 ± 0.436	−0.184 (0.090)	**0.041**	−0.116 (0.066)	0.079
Major rim disk length (mm)	0.630 ± 0.066	0.613 ± 0.063	0.600 ± 0.075	−0.032 (0.015)	**0.039**	−0.018 (0.011)	0.112
Minor rim disk length (mm)	0.619 ± 0.065	0.599 ± 0.062	0.590 ± 0.072	−0.030 (0.015)	**0.042**	−0.021 (0.011)	0.055
Average slope disk diameter (mm)	0.663 ± 0.119	0.653 ± 0.152	0.771 ± 0.136	0.104 (0.028)	**<0.001**	−0.012 (0.025)	0.626
Slope disk area (mm^2)	0.361 ± 0.131	0.358 ± 0.180	0.486 ± 0.164	0.120 (0.032)	**<0.001**	−0.005 (0.028)	0.858
Major slope disk length (mm)	0.068 ± 0.025	0.068 ± 0.034	0.090 ± 0.029	0.021 (0.006)	**<0.001**	$-4.8e^{-4}$ (0.005)	0.930
Minor slope disk length (mm)	0.053 ± 0.019	0.052 ± 0.026	0.072 ± 0.026	0.019 (0.005)	**<0.001**	−0.001 (0.004)	0.772
Average pit flat disk diameter (mm)	0.215 ± 0.030	0.211 ± 0.039	0.257 ± 0.052	0.042 (0.008)	**<0.001**	−0.005 (0.006)	0.440
Pit flat disk area (mm^2)	0.037 ± 0.010	0.036 ± 0.015	0.054 ± 0.025	0.017 (0.003)	**<0.001**	−0.001 (0.002)	0.691
Major pit flat disk length (mm)	0.0067 ± 0.0018	0.0065 ± 0.0027	0.0098 ± 0.0048	0.0032 (0.0007)	**<0.001**	−0.0001 (0.0004)	0.725
Minor pit flat disk length (mm)	0.0058 ± 0.0016	0.0056 ± 0.0023	0.0083 ± 0.0036	0.0026 (0.0005)	**<0.001**	−0.0002 (0.0004)	0.628
Rim volume (mm^3)	1.045 ± 0.153	0.983 ± 0.133	0.910 ± 0.170	−0.141 (0.036)	**<0.001**	−0.061 (0.025)	**0.013**
Inner rim volume (mm^3)	0.104 ± 0.018	0.103 ± 0.019	0.088 ± 0.015	−0.017 (0.004)	**<0.001**	−0.001 (0.003)	0.753
Pit volume (mm^3)	0.252 ± 0.043	0.246 ± 0.051	0.259 ± 0.044	0.005 (0.010)	0.606	−0.007 (0.008)	0.402
Average maximum pit slope (degrees)	12.16 ± 3.38	11.10 ± 2.41	9.86 ± 3.11	−2.42 (0.74)	**0.001**	−1.03 (0.52)	**0.047**

Abbreviations: B = estimate; HC = healthy controls; MS = patients with MS; NMOSD = patients with neuromyelitis optica spectrum disorders; SE = standard error of B.
Significant *p* values are marked in bold.

Table 3 shows the results of this selection process, ordered by AUC. The best parameter selected from the ROC analysis was pit flat disk area (AUC = 0.798, figure 2A). To derive a final set of relevant parameters, we computed a stepwise logistic regression model to predict NMOSD vs MS, including only the parameters with AUC ≥0.7. This selected 4 parameters: pit flat disk area, average pit flat disk diameter, inner rim volume, and major slope disk length (figure 2, D–G).

Association with ON and neuroaxonal damage

A crucial question is whether these parameters react to ON-related damage or are indeed at least partially independent. To further investigate this, we repeated the AUC analysis, but this time separately for the eyes without a history of ON (ON−) and the ON+ (table e-2, links.lww.com/NXI/A271). Indeed, foveal shape was altered also in the ON−. Here, the best foveal shape parameter to distinguish ON− from patients with NMOSD and patients with MS was minor pit flat disk length (AUC = 0.804, figure 2B). In ON+, the best-performing parameter to discriminate between patients with NMOSD and patients with MS was major pit flat disk length (AUC = 0.817, figure 2C). Of note, NMOSD ON− also showed signs of mild neuroaxonal damage compared with HC (pRNFL: B [SE] = −5.7 [2.4] µm, $p = 0.017$; GCIPL: B [SE] = −0.12 [0.04] mm^3, $p = 0.001$).

Table 3 AUC and linear regression analysis results for NMOSD vs MS, sorted in ascending order of AUC

		Linear regression with interaction effects of diagnosis and ON history							
		MS vs NMOSD		ON− vs ON+		NMOSD × ON			
	NMOSD vs MS (AUC)	B (SE)	*p*	B (SE)	*p*	B (SE)	*p*	R^2_{Marg}	R^2_{Cond}
Pit flat disk area (mm²)	**0.798**	0.011 (0.005)	**0.021**	0.001 (0.002)	0.544	0.015 (0.004)	**0.001**	0.176	0.843
Average pit flat disk diameter (mm)	**0.796**	0.033 (0.011)	**0.002**	0.004 (0.005)	0.423	0.029 (0.009)	**0.002**	0.200	0.876
Minor pit flat disk length (mm)	**0.796**	0.0018 (0.0007)	**0.011**	0.0002 (0.0003)	0.645	0.0020 (0.0007)	**0.007**	0.172	0.827
Major pit flat disk length (mm)	**0.790**	0.0019 (0.0009)	**0.038**	0.0003 (0.0004)	0.456	0.0031 (0.0008)	**<0.001**	0.177	0.855
Inner rim volume (mm³)	**0.755**	−0.012 (0.004)	**0.006**	−0.002 (0.001)	0.170	−0.007 (0.003)	**0.006**	0.144	0.940
Minor slope disk length (mm)	**0.744**	0.017 (0.006)	**0.013**	0.001 (0.002)	0.554	0.008 (0.004)	0.051	0.111	0.941
Slope disk area (mm²)	**0.739**	0.102 (0.042)	**0.022**	0.010 (0.011)	0.371	0.053 (0.022)	**0.022**	0.096	0.958
Average slope disk diameter (mm)	**0.739**	0.094 (0.035)	**0.010**	0.006 (0.009)	0.509	0.050 (0.019)	**0.010**	0.116	0.956
Major slope disk length (mm)	**0.733**	0.017 (0.008)	**0.040**	0.002 (0.002)	0.265	0.010 (0.004)	**0.019**	0.083	0.963
Average rim height (mm)	0.664	−0.008 (0.003)	**0.022**	−0.007 (0.002)	**0.001**	−0.009 (0.004)	**0.022**	0.107	0.882
Rim volume (mm³)	0.627	−0.053 (0.032)	0.124	−0.061 (0.016)	**<0.001**	−0.044 (0.032)	0.164	0.081	0.878
Average pit depth (mm)	0.602	−0.007 (0.005)	0.147	−0.007 (0.002)	**<0.001**	−0.009 (0.004)	**0.025**	0.069	0.931
Pit volume (mm³)	0.594	0.012 (0.011)	0.369	−0.006 (0.004)	0.239	0.002 (0.008)	0.845	0.013	0.917
Average maximum pit slope (degrees)	0.593	−0.74 (0.59)	0.210	−0.73 (0.26)	**0.008**	−1.24 (0.51)	**0.019**	0.073	0.908
Major rim disk length (mm)	0.556	−0.010 (0.015)	0.671	−0.021 (0.006)	**0.002**	−0.005 (0.013)	0.697	0.025	0.902
Average rim disk diameter (mm)	0.550	−0.014 (0.026)	0.657	−0.039 (0.012)	**0.002**	−0.010 (0.023)	0.657	0.027	0.891
Rim disk area (mm²)	0.549	−0.043 (0.088)	0.628	−0.128 (0.039)	**0.002**	−0.038 (0.077)	0.628	0.027	0.892
Minor rim disk length (mm)	0.545	−0.004 (0.015)	0.761	−0.022 (0.007)	**0.002**	−0.008 (0.013)	0.756	0.029	0.878
Central foveal thickness (mm)	0.543	−0.001 (0.004)	0.891	$1.5e^{-4}$ (0.001)	0.891	−0.001 (0.002)	0.891	0.002	0.946

Abbreviations: AUC = area under the curve; B = estimate; MS = patients with MS; NMOSD = patients with neuromyelitis optica spectrum disorders; NMOSD × ON = interaction effect of diagnosis and ON; ON = optic neuritis; ON− = eyes without a history of ON; ON+ = eyes with a history of ON; SE = standard error of B; R^2_{Cond} = conditional R-squared; R^2_{Marg} = marginal R-squared.
Significant *p* values and AUC ≥0.7 are marked in bold.

Foveal changes may also be driven not by ON per se, but by the amount of neuroaxonal damage after ON. Here, MS may be a problematic control group because the amount of ON-related retinal damage is typically lesser than in NMOSD.[10,24] To investigate whether differences in neuroaxonal damage are indeed able to explain the observed foveal differences, we repeated the linear regression model analyses for the previously selected 4 parameters, but this time corrected additionally for GCIPL and INL (table 4), which can be considered sensitive parameters for ON severity. Here, it was confirmed that the observed group differences are unlikely to be explained by ON severity differences alone.

See supplemental data for more results on regression analysis corrected for the neuroaxonal damage (table e-3, links.lww.com/NXI/A272). Figure 2, H–I shows rim volume and average pit depth as example foveal shape parameters significantly dependent on ON status but not on diagnosis. Figure 2,

Figure 2 ROC curves, exploratory data analysis for selected parameters, and sample fovea

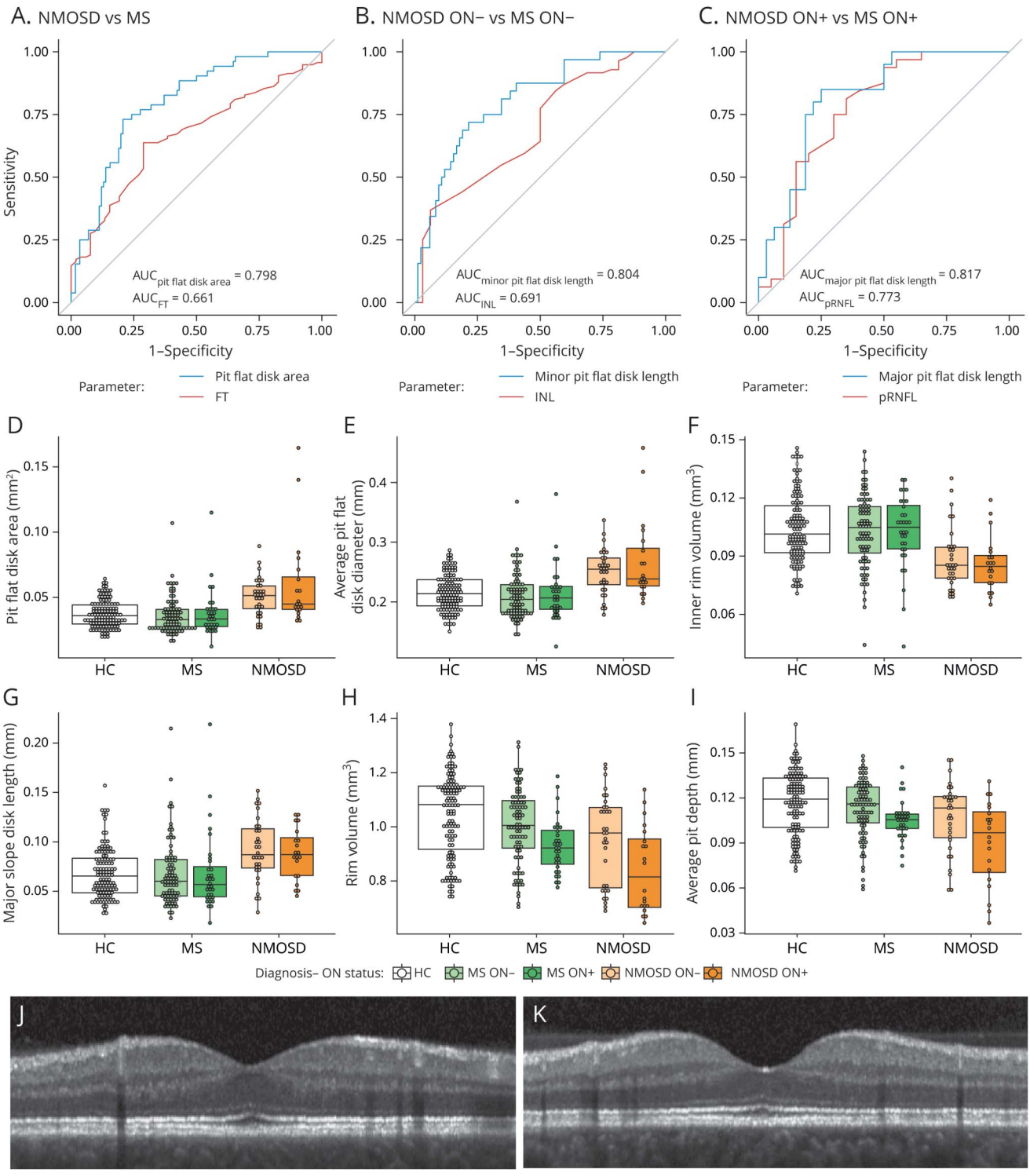

ROC curves for best-performing foveal shape and standard OCT parameters discriminating between (A) NMOSD vs MS, (B) NMOSD ON− vs MS ON−, and (C) NMOSD ON + vs MS ON+. Box and dot plots for (D) pit flat disk area, (E) average pit flat disk diameter, (F) inner rim volume, and (G) major slope disk length, the selected 4 foveal shape parameters. (H) Rim volume and (I) average pit depth, as example foveal shape parameters affected by ON but not diagnosis. A sample central (foveal) B scan of (J) MS ON− and (K) NMOSD ON−, chosen from the median of the selected pit flat disk parameters in each group, demonstrating the difference in foveal pit (pit flat disk), between NMOSD and MS in eyes without a history of ON. AUC = area under the curve; FT = foveal thickness; pRNFL = peripapillary retinal nerve fiber layer thickness; INL = inner nuclear layer volume; HC = healthy controls; MS = patients with MS; NMOSD = patients with neuromyelitis optica spectrum disorders; ON = optic neuritis; ON− = eyes without a history of ON; ON+ = eyes with a history of ON; ROC = receiver operating characteristic.

Table 4 Linear regression results for the selected foveal shape analysis parameters corrected for GCIPL and INL

	Linear regression with interaction effects of diagnosis and ON history corrected for GCIPL									
	MS vs NMOSD		ON− vs ON+		GCIPL (mm^3)		NMOSD × ON			
	B (SE)	*p*	B (SE)	*p*	B (SE)	*p*	B (SE)	*p*	R^2_{Marg}	R^2_{Cond}
Pit flat disk area (mm^2)	0.010 (0.005)	**0.031**	$-3.2e^{-4}$ (0.002)	0.886	−0.016 (0.006)	**0.010**	0.012 (0.004)	**0.010**	0.212	0.858
Average pit flat disk diameter (mm)	0.030 (0.011)	**0.006**	$-8.3e^{-5}$ (0.005)	0.986	−0.038 (0.013)	**0.006**	0.023 (0.009)	**0.019**	0.230	0.889
Inner rim volume (mm^3)	−0.011 (0.004)	**0.013**	$-7.7e^{-4}$ (0.001)	0.554	0.010 (0.004)	**0.013**	−0.006 (0.003)	**0.038**	0.159	0.945
Major slope disk length (mm)	0.017 (0.008)	0.051	0.002 (0.002)	0.360	$5.5e^{-5}$ (0.006)	0.992	0.010 (0.004)	**0.033**	0.082	0.962
	Linear regression with interaction effects of diagnosis and ON history corrected for INL									
	MS vs NMOSD		**ON− vs ON+**		**INL (mm^3)**		**NMOSD × ON**			
	B (SE)	***p***	**B (SE)**	***p***	**B (SE)**	***p***	**B (SE)**	***p***	R^2_{Marg}	R^2_{Cond}
Pit flat disk area (mm^2)	0.012 (0.005)	**0.017**	0.001 (0.002)	0.771	0.041 (0.024)	0.145	0.013 (0.004)	**0.014**	0.193	0.851
Average pit flat disk diameter (mm)	0.035 (0.011)	**0.005**	0.003 (0.005)	0.482	0.075 (0.054)	0.200	0.027 (0.010)	**0.013**	0.208	0.882
Inner rim volume (mm^3)	−0.012 (0.004)	**0.009**	−0.002 (0.001)	0.212	0.003 (0.018)	0.860	−0.008 (0.003)	**0.009**	0.143	0.939
Major slope disk length (mm)	0.016 (0.008)	0.061	0.002 (0.002)	0.312	−0.014 (0.028)	0.623	0.010 (0.004)	**0.022**	0.083	0.962

Abbreviations: B = estimate; GCIPL = combined macular ganglion cell and inner plexiform layer volume; INL = inner nuclear layer volume; MS = patients with MS; NMOSD = patients with neuromyelitis optica spectrum disorders; NMOSD × ON = interaction effect of diagnosis and ON; ON = optic neuritis; ON− = eyes without a history of ON; ON+ = eyes with a history of ON; SE = standard error of B; R^2_{Cond} = conditional R-squared; R^2_{Marg} = marginal R-squared.
Significant *p* values are marked in bold.

J–K shows sample central B scans (crossing the fovea) of ON− from patients with NMOSD and MS, chosen from the median of the selected pit flat disk parameters in each group.

Parameter confirmation

Finally, we tested whether the parameters identified in the exploratory analysis could be confirmed in an independent cohort of patients with NMOSD and MS measured with the same device and protocol at an independent center. Based on differences in the selected parameters, we determined the minimum sample size for a confirmatory cohort as n = 38, 29, 35, and 59 eyes per group, based on measurements for pit flat disk area, average pit flat disk diameter, inner rim volume, and major slope disk length, respectively. In this confirmatory cohort, pit flat disk area and average pit flat disk diameter were confirmed to be significantly different in NMOSD in comparison to MS (B [SE] = 0.007 [0.004] mm^2, $p = 0.035$ and B [SE] = 0.018 [0.010] mm, $p = 0.039$, respectively), neither dependent on ON ($p = 0.254$ and 0.184) nor on NMOSD-specific ON ($p = 0.293$ and 0.382). Differences in inner rim volume were not significant in the confirmatory cohort (diagnosis: $p = 0.125$; ON: $p = 0.080$; NMOSD-specific ON: $p = 0.056$). Major slope disk length only showed a significant association with NMOSD-specific ON (diagnosis: $p = 0.155$; ON history: $p = 0.370$; NMOSD-specific ON: B [SE] = 0.012 [0.007] mm, $p = 0.046$).

Discussion

Using a novel foveal morphometry approach, we here show that foveal shape is altered in patients with AQP4-IgG–seropositive NMOSD. Our results further support that these changes cannot be explained by neuroaxonal damage resulting from ON alone.

Foveal morphometry described a flatter and wider fovea in AQP4-IgG–seropositive NMOSD both in comparison to MS and HC (figure 2, J–K). This is characterized by increased pit flat disk area, increased average pit flat disk diameter, reduced inner rim volume, and increased major slope disk length. Although neuroaxonal damage from ON altered the foveal shape as well, we observed robust changes in these parameters also in eyes never experiencing an ON and when correcting for ON or neuroaxonal damage in the statistical models in all eyes.

The foveal shape changes in AQP4-IgG–seropositive NMOSD reported in our study are supported by previous studies, which investigated thickness or volume changes as indirect evidence for foveal shape changes. Jeong et al.[16] and Oertel et al.[17] showed a significant reduction in FT in eyes of patients with AQP4-IgG–seropositive NMOSD independent of ON in comparison to HCs.

A pathophysiologic explanation for the observed changes could be the presence of a primary retinopathy in AQP4-IgG–seropositive NMOSD, mediated by AQP4-IgG. The principal glial cell of the retina is the Müller cell, expresses AQP4, and is enriched around the fovea.[25] Müller cell bodies reside in the INL, but process stretch through the whole thickness of the retina, linking retinal neurons and photoreceptors with blood vessels. Importantly, animal studies have shown complement-independent AQP4 loss in Müller cells in rats induced by AQP4-IgG, which is in line with an AQP4-IgG–mediated primary retinopathy in NMOSD.[26,27] AQP4-IgG–mediated primary retinal astrocytopathy has been also suggested in human by AQP4-IgG–seropositive NMOSD autopsy cases.[28] AQP4 is expressed in Müller cell end feet—analogous to astrocytic end feet—at the blood-retina barrier.[29] For AQP4-IgG circulating in serum to reach its antigen, the blood-retina barrier presumably needs to be disrupted. Blood-retina or -brain barrier disruptions are typically associated with an acute inflammatory event and then conceptionally linked to an acute attack involving complement.[30] It is unclear whether or to which extent blood-retina/brain barrier disruptions occur in NMOSD and other diseases that do not lead to full attack cascades. A recent analysis of the NMOSD momentum trial data[31] revealed that elevated glial fibrillary acidic protein levels in serum were associated with an increased attack risk, independently suggesting that there is indeed subclinical astrocyte damage outside attacks (Annual European Committee for Treatment and Research in Multiple Sclerosis [ECTRIMS] 2019, P1609).[32] A recent study could further show that in rats, blood-brain barrier breakdown is not necessary for NMOSD pathology, but that NMOSD-like disease can be caused by AQP4-IgG circulating in CSF.[33] We recently reported progressive GCIPL loss without ON in a longitudinal study investigating an overlapping cohort.[34] Further evidence for a primary retinopathy comes from Tian et al.[35] reporting inner retinal layer thinning independent from ON. Significant changes in vascularization of the fovea were also shown in patients with AQP4-IgG–seropositive NMOSD in comparison to HCs using OCT angiography.[36–38]

Alternatively, foveal changes could be caused by subclinical ON. Occasionally, studies have reported neuroaxonal damage also in eyes without prior ON in AQP4-IgG–seropositive NMOSD, which could be interpreted as evidence as such.[39] However, earlier studies had cohort heterogeneity due to incomplete antibody characterization or inclusion of patients with antibody-negative NMOSD. Furthermore, ON in NMOSD often occurs near the chiasm, and neuroaxonal damage can be caused by chiasmal crossover from an affected eye to the fellow eye,[40] which might not be clinically apparent. In this study, we found evidence of neuroaxonal damage also in eyes reported to have never experienced ON, which is in agreement with our recent findings in a multicenter study.[34] It is possible that our data set also included fellow eyes that were affected from cross-chiasmal affects during a contralateral ON. The number of patients with NMOSD only experiencing transverse myelitis and no ON was too small, which is why we refrained from analyzing eyes of these patients separately. In consequence, we cannot fully determine to which extent the observed changes may be caused or affected by covert ON and neuroaxonal damage of the optic nerve.

The main limitation of our study was the low sample size for AQP4-IgG–seropositive NMOSD, especially for patients without a history of ON, which is unfortunately common in studies investigating NMOSD. Another limitation of this study is that the diagnostic value is unclear, as we only used scans from 1 OCT device using a single scanning protocol. It is unclear how scans from different OCT devices and scanning protocols can be compared.

Foveal morphometry may potentially be useful for differential diagnosis of AQP4-IgG–seropositive NMOSD. Typically, pRNFL and GCIPL as well as other OCT parameters associated with neuroaxonal damage are mostly nonspecific to the underlying ON etiology. In contrast, many foveal morphometry parameters showed significant differences between patients with NMOSD and MS in this study. Parameter selection resulted in 4 promising parameters describing foveal differences: pit flat disk area, average pit flat disk diameter, major slope disk length, and inner rim volume. Only the first 2 parameters could be confirmed in an independent cohort. The reason may be the different frequency of ON in the confirmatory cohort between patients with MS and NMOSD, which exemplifies the need for additional confirmation, especially in eyes that are inconspicuous in regard to neuroaxonal damage from ON. Future work should further investigate this by comparing patients with myelin oligodendrocyte glycoprotein (MOG)-IgG–seropositive disease against patients with MOG/AQP4-IgG double-negative NMOSD, as well as clarify effects of scan protocols and foveal variability in healthy persons.

Study funding

Supported by the Einstein Foundation Berlin (Einstein Junior Scholarship to S.M.), the German Federal Ministry of Economic Affairs and Energy (BMWI EXIST 03EFEBE079 to A.U.B. and E.M.K.), German Research Foundation (DFG Exc. 257 to F.P. and A.U.B.), German Federal Ministry of Education and Research (BMBF Neu^2 ADVISIMS to F.P. and A.U.B. as well as part of the "German Competence Network Multiple Sclerosis" (KKNMS), project NationNMO, 01GI1602B to O.A.), and Novartis (research grant to H.G.Z.).

Disclosure

E.M. Kadas, S.K. Yadav, A.U. Brandt, S. Motamedi, and F. Paul are named as coinventors on the patent application for the foveal shape analysis method used by this manuscript ("Method for estimating shape parameters of the fovea by optical coherence tomography", International Publication Number: "WO 2019/016319 A1"). E.M. Kadas, S.K. Yadav, F. Paul, and A.U. Brandt are cofounders and hold shares in technology start-up Nocturne GmbH, which has commercial interest in OCT applications in neurology. E.M. Kadas and S.K. Yadav are now employees of Nocturne GmbH. H.G. Zimmermann received a research grant from Novartis. All other authors report no relevant disclosures. Go to Neurology.org/NN for full disclosures.

Publication history

Received by *Neurology: Neuroimmunology & Neuroinflammation* January 30, 2020. Accepted in final form April 16, 2020.

Appendix Authors

Name	Location	Contribution
Seyedamirhosein Motamedi, MSc	Charité—Universitätsmedizin Berlin, Germany	Collected the data; conducted the statistical analysis; contributed to development of the foveal shape analysis method; and drafted the manuscript for intellectual content
Frederike C. Oertel, MD	Charité—Universitätsmedizin Berlin, Germany	Collected the data; performed OCT quality control and segmentation; contributed to data interpretation; and revised the manuscript for intellectual content
Sunil K. Yadav, PhD	Charité—Universitätsmedizin Berlin, Germany	Developed the foveal shape analysis method and revised the manuscript for intellectual content
Ella M. Kadas, PhD	Charité—Universitätsmedizin Berlin, Germany	Contributed to development of the foveal shape analysis method and revised the manuscript for intellectual content
Margit Weise, MSc	Heinrich Heine University, Düsseldorf, Germany	Major role in acquisition of the confirmatory data and revised the manuscript for intellectual content
Joachim Havla, MD	Ludwig-Maximilians University, Munich, Germany	Contributed to data interpretation and revised the manuscript for intellectual content
Marius Ringelstein, MD	Heinrich Heine University, Düsseldorf, Germany	Major role in acquisition of the confirmatory data and revised the manuscript for intellectual content
Orhan Aktas, MD	Heinrich Heine University, Düsseldorf, Germany	Major role in acquisition of the confirmatory data and revised the manuscript for intellectual content
Philipp Albrecht, MD	Heinrich Heine University, Düsseldorf, Germany	Major role in acquisition of the confirmatory data and revised the manuscript for intellectual content
Klemens Ruprecht, MD	Charité—Universitätsmedizin Berlin, Germany	Contributed to study management and revised the manuscript for intellectual content
Judith Bellmann-Strobl, MD	Charité—Universitätsmedizin Berlin, Germany	Contributed to study management and revised the manuscript for intellectual content
Hanna G. Zimmermann, PhD	Charité—Universitätsmedizin Berlin, Germany	Contributed to data interpretation and revised the manuscript for intellectual content
Friedemann Paul, MD	Charité—Universitätsmedizin Berlin, Germany	Contributed to study management; contributed to data interpretation; and revised the manuscript for intellectual content
Alexander U. Brandt, MD	Charité—Universitätsmedizin Berlin, Germany	Designed and conceptualized the study; supervised the statistical analysis; and drafted the manuscript for intellectual content

References

1. Jarius S, Paul F, Franciotta D, et al. Mechanisms of disease: aquaporin-4 antibodies in neuromyelitis optica. Nat Clin Pract Neurol 2008;4:202–214.
2. Paul F, Jarius S, Aktas O, et al. Antibody to aquaporin 4 in the diagnosis of neuromyelitis optica. PLoS Med 2007;4:e133.
3. Zekeridou A, Lennon VA. Aquaporin-4 autoimmunity. Neurol Neuroimmunol Neuroinflamm 2015;2:e110. doi: 10.1212/NXI.0000000000000110.
4. Jarius S, Wildemann B, Paul F. Neuromyelitis optica: clinical features, immunopathogenesis and treatment: neuromyelitis optica. Clin Exp Immunol 2014;176:149–164.
5. Schmidt F, Zimmermann H, Mikolajczak J, et al. Severe structural and functional visual system damage leads to profound loss of vision-related quality of life in patients with neuromyelitis optica spectrum disorders. Mult Scler Relat Disord 2017;11:45–50.
6. Schneider E, Zimmermann H, Oberwahrenbrock T, et al. Optical coherence tomography reveals distinct patterns of retinal damage in neuromyelitis optica and multiple sclerosis. PLoS One 2013;8:e66151.
7. Wingerchuk DM, Banwell B, Bennett JL, et al. International consensus diagnostic criteria for neuromyelitis optica spectrum disorders. Neurology 2015;85:177–189.
8. Yamamura T, Nakashima I. Foveal thinning in neuromyelitis optica: a sign of retinal astrocytopathy? Neurol Neuroimmunol Neuroinflamm 2017;4:e347. doi: 10.1212/NXI.0000000000000347.
9. Oertel FC, Zimmermann H, Paul F, Brandt AU. Optical coherence tomography in neuromyelitis optica spectrum disorders: potential advantages for individualized monitoring of progression and therapy. EPMA J 2018;9:21–33.
10. Bennett JL, de Seze J, Lana-Peixoto M, et al. Neuromyelitis optica and multiple sclerosis: seeing differences through optical coherence tomography. Mult Scler Houndmills Basingstoke Engl 2015;21:678–688.
11. Oertel FC, Zimmermann H, Mikolajczak J, et al. Contribution of blood vessels to retinal nerve fiber layer thickness in NMOSD. Neurol Neuroimmunol Neuroinflamm 2017;4:e338. doi: 10.1212/NXI.0000000000000338.
12. Oberwahrenbrock T, Traber GL, Lukas S, et al. Multicenter reliability of semiautomatic retinal layer segmentation using OCT. Neurol Neuroimmunol Neuroinflamm 2018;5:e449. doi: 10.1212/NXI.0000000000000449.
13. Kaufhold F, Zimmermann H, Schneider E, et al. Optic neuritis is associated with inner nuclear layer thickening and microcystic macular edema independently of multiple sclerosis. PLoS One 2013;8:e71145.
14. Syc SB, Saidha S, Newsome SD, et al. Optical coherence tomography segmentation reveals ganglion cell layer pathology after optic neuritis. Brain 2012;135:521–533.
15. Pache F, Zimmermann H, Mikolajczak J, et al. MOG-IgG in NMO and related disorders: a multicenter study of 50 patients. Part 4: afferent visual system damage after optic neuritis in MOG-IgG-seropositive versus AQP4-IgG-seropositive patients. J Neuroinflammation 2016;13:282.
16. Jeong IH, Kim HJ, Kim NH, Jeong KS, Park CY. Subclinical primary retinal pathology in neuromyelitis optica spectrum disorder. J Neurol 2016;263:1343–1348.
17. Oertel FC, Kuchling J, Zimmermann H, et al. Microstructural visual system changes in AQP4-antibody–seropositive NMOSD. Neurol Neuroimmunol Neuroinflamm 2017;4:e334. doi: 10.1212/NXI.0000000000000334.
18. Yadav SK, Motamedi S, Oberwahrenbrock T, et al. CuBe: parametric modeling of 3D foveal shape using cubic Bézier. Biomed Opt Express 2017;8:4181.
19. Tewarie P, Balk L, Costello F, et al. The OSCAR-IB consensus criteria for retinal OCT quality assessment. PLoS One 2012;7:e34823.
20. Polman CH, Reingold SC, Banwell B, et al. Diagnostic criteria for multiple sclerosis: 2010 revisions to the McDonald criteria. Ann Neurol 2011;69:292–302.
21. Schippling S, Balk LJ, Costello F, et al. Quality control for retinal OCT in multiple sclerosis: validation of the OSCAR-IB criteria. Mult Scler Houndmills Basingstoke Engl 2015;21:163–170.
22. Cruz-Herranz A, Balk LJ, Oberwahrenbrock T, et al. The APOSTEL recommendations for reporting quantitative optical coherence tomography studies. Neurology 2016;86:2303–2309.
23. R Core Team. R: A Language and Environment for Statistical Computing [online]. Vienna: R Foundation for Statistical Computing; 2018. Available at: www.R-project.org/. Accessed June 13, 2019.
24. Ratchford JN, Quigg ME, Conger A, et al. Optical coherence tomography helps differentiate neuromyelitis optica and MS optic neuropathies. Neurology 2009;73:302–308.
25. Bringmann A, Pannicke T, Grosche J, et al. Müller cells in the healthy and diseased retina. Prog Retin Eye Res 2006;25:397–424.
26. Felix CM, Levin MH, Verkman AS. Complement-independent retinal pathology produced by intravitreal injection of neuromyelitis optica immunoglobulin G. J Neuroinflammation 2016;13:275.
27. Zeka B, Hastermann M, Kaufmann N, et al. Aquaporin 4-specific T cells and NMO-IgG cause primary retinal damage in experimental NMO/SD. Acta Neuropathol Commun 2016;4:82.
28. Hokari M, Yokoseki A, Arakawa M, et al. Clinicopathological features in anterior visual pathway in neuromyelitis optica. Ann Neurol 2016;79:605–624.
29. Goodyear MJ, Crewther SG, Junghans BM. A role for aquaporin-4 in fluid regulation in the inner retina. Vis Neurosci 2009;26:159–165.
30. Takeshita Y, Obermeier B, Cotleur AC, et al. Effects of neuromyelitis optica-IgG at the blood-brain barrier in vitro. Neurol Neuroimmunol Neuroinflamm 2017;4:e311. doi: 10.1212/NXI.0000000000000311.
31. Cree BAC, Bennett JL, Kim HJ, et al. Inebilizumab for the treatment of neuromyelitis optica spectrum disorder (N-MOmentum): a double-blind, randomised placebo-controlled phase 2/3 trial. Lancet Lond Engl 2019;394:1352–1363.
32. ECTRIMS 2019—late breaking news abstracts. Mult Scler J 2019;25:890–938.

33. Hillebrand S, Schanda K, Nigritinou M, et al. Circulating AQP4-specific autoantibodies alone can induce neuromyelitis optica spectrum disorder in the rat. Acta Neuropathol (Berl) 2019;137:467–485.
34. Oertel FC, Havla J, Roca-Fernández A, et al. Retinal ganglion cell loss in neuromyelitis optica: a longitudinal study. J Neurol Neurosurg Psychiatry 2018;89:1259–1265.
35. Tian DC, Su L, Fan M, et al. Bidirectional degeneration in the visual pathway in neuromyelitis optica spectrum disorder (NMOSD). Mult Scler J 2018;24:1585–1593.
36. Huang Y, Zhou L, ZhangBao J, et al. Peripapillary and parafoveal vascular network assessment by optical coherence tomography angiography in aquaporin-4 antibody-positive neuromyelitis optica spectrum disorders. Br J Ophthalmol 2019;103:789–796.
37. Kwapong WR, Peng C, He Z, Zhuang X, Shen M, Lu F. Altered macular microvasculature in neuromyelitis optica spectrum disorders. Am J Ophthalmol 2018;192:47–55.
38. Green AJ, Cree BAC. Distinctive retinal nerve fibre layer and vascular changes in neuromyelitis optica following optic neuritis. J Neurol Neurosurg Psychiatry 2009;80:1002–1005.
39. Ringelstein M, Harmel J, Zimmermann H, et al. Longitudinal optic neuritis-unrelated visual evoked potential changes in NMO spectrum disorders. Neurology 2020;94:e407–e418.
40. Ramanathan S, Prelog K, Barnes EH, et al. Radiological differentiation of optic neuritis with myelin oligodendrocyte glycoprotein antibodies, aquaporin-4 antibodies, and multiple sclerosis. Mult Scler Houndmills Basingstoke Engl 2016;22:470–482.

Curriculum Vitae

Mein Lebenslauf wird aus datenschutzrechtlichen Gründen in der elektronischen Version meiner Arbeit nicht veröffentlicht.

My curriculum vitae does not appear in the electronic version of my paper for reasons of data protection.

List of Publications

Journal Articles

Motamedi, S.; Gawlik, K.; Ayadi, N.; Zimmermann, H.G.; Asseyer, S.; Bereuter, C.; Mikolajczak, J.; Paul, F.; Kadas, E.M.; Brandt, A.U. Normative Data and Minimally Detectable Change for Inner Retinal Layer Thicknesses Using a Semi-Automated OCT Image Segmentation Pipeline. Frontiers in Neurology, 2019.
Journal Impact Factor (2019): 2.889

Motamedi, S.; Oertel, F.C.; Yadav, S.K.; Kadas, E.M.; Weise, M.; Havla, J.; Ringelstein, M.; Aktas, O.; Albrecht, P.; Ruprecht, K.; Bellmann-Strobl, J.; Zimmermann, H.G.; Paul, F.; Brandt A.U. Altered fovea in AQP4-IgG-seropositive neuromyelitis optica spectrum disorders. Neurology-Neuroimmunology & Neuroinflammation, 2020.
Journal Impact Factor (2019): 7.724

Yadav, S.K.; **Motamedi, S.**; Oberwahrenbrock, T.; Oertel, F.C.; Polthier, K.; Paul, F.; Kadas, E.M.; Brandt, A.U. CuBe: Parametric Modeling of 3D Foveal Shape Using Cubic Bézier. Biomedical Optical Express, 2017.
Journal Impact Factor (2019): 3.921

Yadav, S.K.; Kadas, E.M.; **Motamedi, S.**; Polthier, K.; Haußer, F.; Gawlik, K.; Paul, F.; Brandt, A.U. Optic nerve head three-dimensional shape analysis. Journal of Biomedical Optics, 2018.
Journal Impact Factor (2019): 2.785

Ayadi, N.; Dörr, J.; **Motamedi, S.**; Gawlik, K.; Bellmann-Strobl, J.; Mikolajczak, J.; Brandt, A.U.; Zimmermann, H.; Paul, F. Temporal Visual Resolution and Disease Severity in MS. Neurology-Neuroimmunology & Neuroinflammation, 2018.
Journal Impact Factor (2019): 7.724

Oertel, F.C.; Zeitz, O.; Rönnefarth, M.; Bereuter, C.; **Motamedi, S.**; Zimmermann, H.G.; Kuchling, J.; Grosch, A.S.; Doss, S.; Browne, A.; Paul, F.; Schmitz-Hübsch, T.; Brandt, A.U. Functionally Relevant Maculopathy and Optic Atrophy in Spinocerebellar Ataxia Type 1. Movement Disorders Clinical Practice, 2020.
Journal Impact Factor (2019): -

Oertel, F.C.; Havla, J.; Roca-Fernández, A.; Lizak, N.; Zimmermann, H.; **Motamedi, S.**; Borisow, N.; White, O.B.; Bellmann-Strobl, J.; Albrecht, P.; Ruprecht, K.; Jarius, S.; Palace, J.; Leite, M.I.;

Kümpfel, T.; Paul, F.; Brandt, A.U. Retinal ganglion cell loss in neuromyelitis optica: a longitudinal study. Journal of Neurology, Neurosurgery & Psychiatry, 2018.
Journal Impact Factor (2019): 8.234

Conference Contributions

Motamedi, S.; Oertel, F.C.; Yadav, S.; Kadas, E.M.; Ruprecht, K.; Bellmann-Strobl, J.; Zimmermann, H.G.; Paul, F.; Brandt, A.U. Foveal Shape Differs Between Neuromyelitis Optica and Multiple Sclerosis Patients. Poster presentation at the annual meeting of the American Academy of Neurology (online), Toronto, Canada, 2020.

Motamedi, S.; Oertel, F.C.; Yadav, S.; Siebert, N.; Bellmann-Strobl, J.; Ruprecht, K.; Kadas, E.M.; Paul, F.; Zimmermann, H.G.; Brandt, A.U. Altered optic nerve head morphology in aquaporin-4 igg seropositive neuromyelitis optica. Poster presentation at the annual meeting of the European Committee for Treatment and Research in Multiple Sclerosis (ECTRIMS), Stockholm, Sweden, 2019.

Motamedi, S.; Oertel, F.C.; Havla, J.; Yadav, S.; Kadas, E.M.; Zimmermann, H.G.; Ruprecht, K.; Bellmann-Strobl, J.; Kümpfel, T.; Paul, F.; Brandt, A.U. 3D fovea morphometry reveals distinct foveal changes in neuromyelitis optica spectrum disorders. Poster presentation at the annual meeting of the European Committee for Treatment and Research in Multiple Sclerosis (ECTRIMS), Berlin, Germany, 2018.

Oertel, F.C.; Specovius, S.; Zimmermann, H.G.; Chien, C.; **Motamedi, S.**; Cook, L.; Martinez-Lapiscina, E.H.; Lana Peixoto, M.A.; Fontenelle, M.A.; Palace, J.; Roca-Fernandez, A.; Siritho, S.; Altintas, A.; Tanriverdi, U.; Jacob, A.; Huda, S.; Marignier, R.; Nerrant, E.; Cobo Calvo, A.; de Sèze, J.; Senger, T.; Pandit, L.; Dcunha, A.; de Castillo, I.S.; Bichuetti, D.; Tavares, M.; May, E.F.; Tongco, C.; Havla, J.; Leocani, L.; Pisa, M.; Ashtari, F.; Kafieh, R.; Aktas, O.; Ringelstein, M.; Albrecht, P.; Kim, H.J.; Hyun, J.-W.; Asgari, N.; Soelberg, K.; Mao-Draayer, Y.; Stiebel-Kalish, H.; Rimler, Z.; Reid, A.; Yeaman, M.; Smith, T.J.; Brandt, A.U.; Paul, F.; GJCF International Clinical Consortium for NMOSD. An international retrospective multi-center study of retinal optical coherence tomography in neuromyelitis optica spectrum disorders: the CROCTINO study. Poster presentation at the annual meeting of the European Committee for Treatment and Research in Multiple Sclerosis (ECTRIMS), Stockholm, Sweden, 2019.

Zimmermann, H.G.; Vitkova, V.; Ayadi, N.; Martorell Serra, I.; Bereuter, C.; **Motamedi, S.**; Kuchling, J.; Asseyer, S.; Scheel, M.; Ruprecht, K.; Bellmann-Strobl, J.; Paul, F.; Brandt, A.U. Individual reflection of brain atrophy on intraretinal thickness changes in multiple sclerosis. Poster

presentation at the annual meeting of the European Committee for Treatment and Research in Multiple Sclerosis (ECTRIMS), Stockholm, Sweden, 2019.

Vitkova, V.; Zimmermann, H.; Ayadi, N.; Martorell Serra, I.; Koduah, P.; Chien, C.; Kuchling, J.; Gieß, R.; **Motamedi, S.**; Gawlik, K.; Bellmann-Strobl, J.; Ruprecht, K.; Scheel, M.; Paul, F.; Brandt, A. Quantitative OCT and MRI in MS as surrogates for clinical activity based on annual follow-ups. Poster presentation at the annual meeting of the European Committee for Treatment and Research in Multiple Sclerosis (ECTRIMS), Berlin, Germany, 2018.

Acknowledgements

First of all, I would like to thank everyone who supported me, by any means, in conducting and concluding my doctoral study.

I would like to express my sincere gratitude to my doctoral supervisor, Prof. Friedemann Paul, for his consistent support and guidance during the course this doctorate.

I want to say a special thank you to my supervisor, Dr. Alexander U. Brandt, without whose continued support and guidance, enthusiasm, and valuable inputs, I could not have achieved my goals during this research.

I would also like to thank all my colleagues and coauthors who provided excellent assistance and collaboration, and send a special thanks to Dr. Hanna G. Zimmermann for her superb support and coordination, and valued inputs.

I would also like to thank Einstein Foundation Berlin for financially supporting two years of my doctorate study by granting me Einstein Junior Scholarship.

I want to thank my wife, Setareh Sharifi Panah, for always being by my side during this time.

Lastly yet importantly, I would like to express my deepest gratitude to the patients and participants who patiently participated in our studies and to the countless number of study nurses, technicians, and hospital staff, without whom this would not have been possible.